Quaternary Science Reviews 306 (2023) 108038

Contents lists available at ScienceDirect

Quaternary Science Reviews

journal homepage: www.elsevier.com/locate/quascirev

Timing and extent of late Quaternary glaciations on Karlik Mountain, eastern Tianshan range, China

Jingdong Zhao [a, d, *], Jinkun Qiu [b], Jonathan M. Harbor [c], Huihan Ji [b], Marc W. Caffee [c, e], Wanqin Guo [a], Huijun Zheng [a]

[a] State Key Laboratory of Cryospheric Science, Northwest Institute of Eco-Environment and Resources, Chinese Academy of Sciences, Lanzhou, 730000, China
[b] Key Laboratory of Western China's Environmental Systems (MOE), Lanzhou University, Lanzhou, 730000, China
[c] Department of Earth, Atmospheric, And Planetary Sciences, Purdue University, And Purdue University Global, West Lafayette, 47907, USA
[d] School of Geography, Geomatics, And Planning, Jiangsu Normal University, Xuzhou, 221116, China
[e] Department of Physics and Astronomy, Purdue Rare Isotope Measurement Laboratory (PRIME Lab), Purdue University, West Lafayette, 47907, USA

ARTICLE INFO

Article history:
Received 23 November 2022
Received in revised form
28 February 2023
Accepted 8 March 2023
Available online 16 March 2023

Handling Editor: C. O'Cofaigh

Keywords:
Glacial landform
Terrestrial *in situ* cosmogenic nuclides (TCN)
Late quaternary
Global last glacial maximum (LGM_G)
Tianshan range

ABSTRACT

Glacial landforms formed by multiple glaciations are well-preserved in the valleys around Karlik Mountain in the easternmost Tianshan range, Central Asia. These landforms are direct imprints of palaeoglaciers and represent important archives of past climatic and environmental conditions. Dating these landforms contributes to understanding the spatiotemporal variations of past glaciers and provides key information for reconstructing the palaeoclimate and palaeoenvironment in Central Asia. In this study, thirty-two boulder and bedrock samples were collected from two glaciated valleys on the southern slope of Karlik Mountain for terrestrial *in situ* cosmogenic nuclides (TCN) ^{10}Be surface exposure dating. Based on the geomorphic relationships and dating results, the innermost M_{S1} moraine complex was deposited during the Little Ice Age (LIA); the M_{S2} moraine complex was formed during the Late-glacial; the M_{S3} moraine complex was deposited during the global Last Glacial Maximum (LGM_G); the M_{S4} moraine complex, which is the largest moraine complex, is marine oxygen isotope stage (MIS) 4 in ages; and the M_{S5} moraine complex, which is only preserved at the interfluve ridges, has a similar age to M_{S4}. The age of M_{S4} demonstrates that the largest local last glacial maximum (LGM_L) occurred during the early part of the last glacial cycle rather than during the LGM_G. The M_{S4} and M_{S5} glacial complexes imply that a large ice cap with outlet valley glaciers developed on the whole of Karlik Mountain during MIS 4. These ages, combined with previous landform mapping and dating on the northern slope of the mountain, show that glacial advances since MIS 4 in this mountainous area were restricted to the valleys, rather than large ice cap scale, which is consistent with moraine records in the other valleys across the Tianshan range. The pattern and nearly synchronous timing of palaeoglacier fluctuations during the last glaciation in arid Central Asia imply that the main determinant for glacier fluctuations in this region has been changes in precipitation brought by the westerlies during periods of low temperature.

1. Introduction

Mountain glaciers are sensitive to regional and local climate change (Cuffey and Paterson, 2010), and are active geomorphic agents in shaping the landscapes of the high and cold regions. Glacial erosional and depositional landforms are direct imprints of past glaciations and contain important palaeoclimatic and palaeoenvironmental information (Embleton and King, 1975; Bennett and Glasser, 2009; Benn and Evans, 2010). The timing, extent, properties, and type of past glaciers can be reconstructed using these landforms, which provides insights into past glacier changes, and contributes to understanding palaeoclimate and palaeoenvironment in the study areas (Shi et al., 2006, 2011; Ehlers et al., 2011).

Quantifying the chronology of glacial landforms and deposits is the first step towards understanding the spatiotemporal variations

* Corresponding author. State Key Laboratory of Cryospheric Science, Northwest Institute of Eco-Environment and Resources, Chinese Academy of Sciences, Lanzhou, 730000, China.
E-mail address: jdzhao@lzb.ac.cn (J. Zhao).

https://doi.org/10.1016/j.quascirev.2023.108038
0277-3791/

of glaciers and the landscape evolution in glaciated areas. With the development and refinement of numerical dating techniques, including terrestrial *in situ* cosmogenic nuclides (TCN), optically stimulated luminescence (OSL) and electron spin resonance (ESR), significant progress has been made in Quaternary glaciation research throughout the world (Shi et al., 2006, 2011; Ehlers et al., 2011; Owen and Dortch, 2014). In addition, robust chronological frameworks established with consistent methods, such as TCNs, allow for comparisons of interregional and intraregional glacial events (Dortch et al., 2013; Murari et al., 2014). Regional and global analyses of the pattern, scale, and timing of past glacier fluctuations has also provided insights into climate forcing mechanisms that control glaciation (Schaefer et al., 2006; Clark et al., 2009; Balco, 2011, 2020).

The Tianshan range in Central Asia is a ~2500 km long arc of WSW-ENE trending mountains with many peaks exceeding 5000 m asl. It extends from the western boundary of Kyrgyzstan, across the middle of the Xinjiang Uighur Autonomous Region, China, to near the Mongolian border (Fig. 1). Tens of thousands of modern active glaciers are present on these high peaks, making this highland a key part of the "Water Tower of Central Asia" (Sorg et al., 2012). Meltwater from these glaciers is vital to support rivers and oases, and sustain the development of society, economy and ecology in this very dry region. Distinct, large-scale glacial landforms in the valleys, basins and on the piedmont throughout this mountain system indicate that extensive advances and retreats of glaciers occurred during glacial-interglacial cycles in the Quaternary (Shi et al., 2006). Studies of these landforms help advance our understanding of the spatiotemporal variation of palaeoglaciers, paleoclimate and palaeoenvironment in Central Asia. In the past two decades, progress on glacial chronologies in this range has been made, and palaeoclimatic trends, regional correlations and hemispheric teleconnections, climatic forcing mechanisms behind the palaeoglacier fluctuation have been discussed (Zhou et al., 2002; Yi et al., 2004; Abramowski et al., 2006; Zhao et al., 2006, 2009, 2010, 2012, 2015; Narama et al., 2007, 2009; Koppes et al., 2008; Kong et al., 2009; Xu et al., 2010; Li et al., 2011, 2014, 2016a, 2016b; Zech, 2012; Stroeven et al., 2013; Lifton et al., 2014a; Chen et al., 2015; Ou et al., 2015; Blomdin et al., 2016; Zhang et al., 2016a; Batbaatar et al., 2020; Liu et al., 2021).

Glacial landforms on Karlik Mountain, in the easternmost Tianshan range, have been studied since the 1960s (Hu et al., 1964; Hu, 1979; Wang, 1981, 1986), but early studies were limited by the lack of robust dating techniques at that time. Recently, Chen et al. (2015) used ^{10}Be surface exposure and OSL dating techniques to investigate the glacial landforms in the Turgan Valley on the northern slope of this mountain. Little Ice Age (LIA), Lateglacial, marine oxygen isotope stage (MIS) 3 and MIS 4 or older glacial events were identified, however, some conclusions, such as assignments to LIA and MIS 4 or older glaciations were tentative due to the scatter in the ^{10}Be ages. The timing and extent of late Quaternary glaciations on the southern slope is still unclear, specifically the timing and extent of the global Last Glacial Maximum (LGM_G). These questions need to be solved to fully understand the Quaternary glaciations on Karlik Mountain and the spatiotemporal variations of palaeoclimate and palaeoenvironment in Central Asia. In this study, high-resolution remote-sensing, topographical maps, field observation and mapping, and ^{10}Be surface exposure dating techniques are used to define the timing and extent of the late Quaternary glaciations in the Miaoergou and Yushugou river valleys on the southern slope of Karlik Mountain. In combination with previous ^{10}Be and OSL ages (Chen et al., 2015) from the Turgan River valley on the northern slope, the goal of this study is to provide a reliable chronological framework for late Quaternary glaciations on Karlik Mountain, and to examine connections between paleoglaciation and climate forcing mechanisms.

2. Regional setting

The climate of Karlik Mountain is dominated by the mid-latitude westerlies year-round (Chen et al., 2019) and influenced by the Siberian High in the winter. Regions to the southwest (Hami) and northeast (Yiwu) have a pronounced continental climate. Based on observational data at the 600 hPa level at the Hami weather station, the average summer (June–August) temperature is −0.9 °C and the annual mean temperature is −9 °C (Wang et al., 1986). Based on short-term meteorological observations at the terminus of Halatabudi Glacier (No. 5Y822C-2), combined with meteorological data from surrounding areas, the annual precipitation is estimated to be about 600 mm in the glaciated area, with most precipitation in summer and autumn (Wang et al., 1986).

The setting and topography of Karlik Mountain is suitable for glacier development. The ridges are between 3500 and 4800 m asl, and the highest peak is Tomurty (4886 m asl), which is about 1000 m above local modern equilibrium-line altitude (ELA). According to data provided in the Second Glacier Inventory of China, there were 151 modern active glaciers with an area of 110.06 km^2 and ice volume 5.5499 km^3 on this mountain in 2007 (Guo et al.,

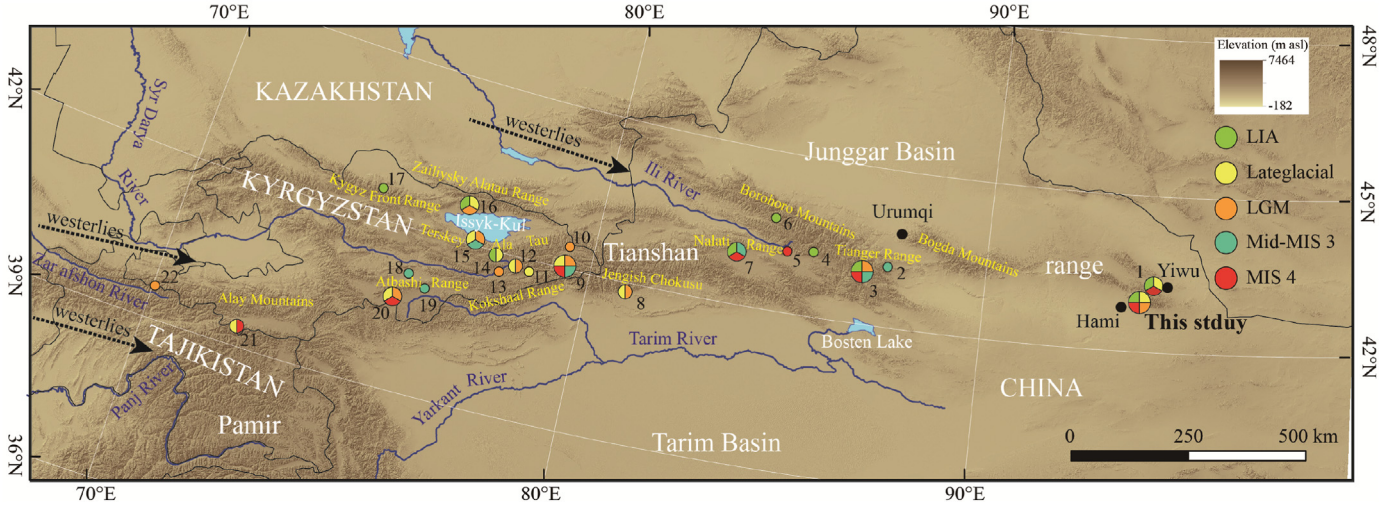

Fig. 1. ^{10}Be dating studies and glacial events across the Tianshan range (detailed information and references for sites No.1 to No.22 are provided in the supplementary materials).

2015; Liu et al., 2015). In comparison, data in the First Glacier Inventory of China showed that 122 glaciers with an area of 125.89 km^2 and ice volume 7.0185 km^3 in 1972 (LIGG, 1986). Thus the glaciers have shrunk and the ice volume has decreased, and some large glaciers have disintegrated into several smaller ones from 1972 to 2007. Most of the remaining large glaciers are on the southern slope, especially in our research area. This asymmetrical distribution occurs as a result of the longer and gentler up-valley longitudinal profiles on the southern slope. Glaciers on Karlik Mountain include flat-top ice caps, valley glaciers, cirque glaciers and hanging glaciers.

Eight small rivers originate on the southern slope of Karlik Mountain and flow southward or southwestward to the Hami Basin, including the Yushugou and the Miaoergou rivers. The total annual discharge of these rivers is 5×10^8 m^3, with 16.4% of this being glacier meltwater (Wang et al., 1986). In our research area, there are 16 glaciers with an area of 41.28 km^2 and an ice volume of 2.8625 km^3 (LIGG, 1986). These glaciers are relatively large and account for 33% of the area and 41% of the ice volume. The Halatabudi Glacier is the largest glacier on Karlik Mountain, with an area of 6.59 km^2 and the ice volume of 0.5404 km^3. It is 6.5 km in length, has a terminus at about 3610 m asl, and extends more than 500 m below its ELA (~4170 m asl) (LIGG, 1986).

3. Glacial landforms

Glacial erosional landforms (including U-shaped valleys, cirques, arêtes, roche moutonnées, and glacially polished surfaces) are well developed and depositional landforms (including end moraines, lateral moraines, ground moraines, and hummocky moraines) are well preserved in the valleys around Karlik Mountain. These landforms record a complex glacial history and landscape evolution on this mountain, and their assemblage demonstrates that several large compound valley glaciers and a large ice cap with many outlet valley glaciers once developed there during past glaciations. Our study focuses on the glacial landforms in the Miaoergou and Yushugou river valleys on the southern slope (Figs. 2 and 3).

3.1. Glacial erosional landforms

The most distinct glacial erosional landforms are well developed U-shaped valleys, commonly they are 3–5 km long, extending to the south or southwest and nearly parallel to each other (Fig. 2a and b). Parts of narrow ridges that separate these troughs are arêtes. Roche moutonnées and glacially polished surfaces occur at the bottom of these glacial troughs. Empty cirques occur along the broad ridges between the adjacent valleys (Fig. 2c).

3.2. Glacial depositional landforms

As a result of recent climate change, glaciers on Karlik Mountain have experienced extensive thinning and retreat. A comparison of topographic maps and high-resolution satellite remote-sensing imagery showed that the glaciers in this area have shrunk, with tens to hundreds of meters of retreat of the termini of these glaciers during 1972–2016, and the ice volume has also decreased rapidly (Yang et al., 2019). A comparison of the satellite remote-sensing

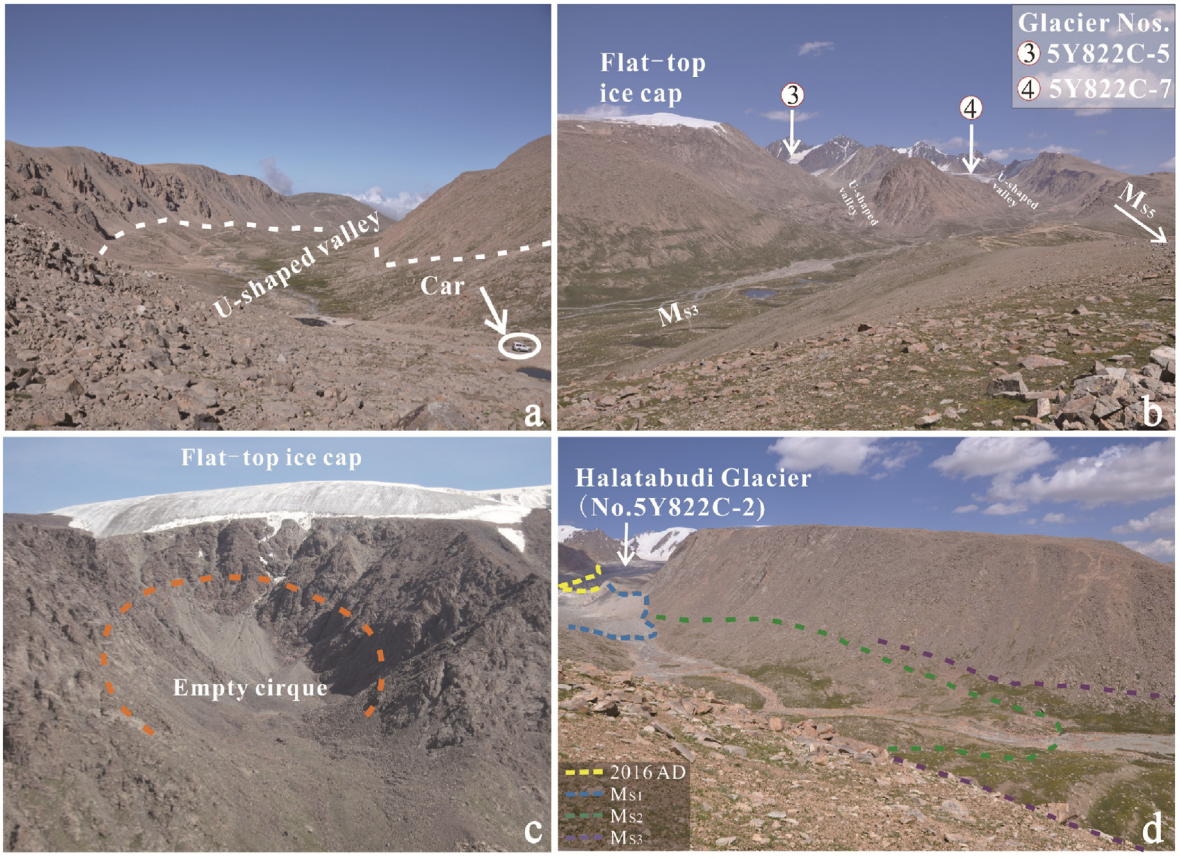

Fig. 2. Representative glacial erosional and depositional landforms in the Miaoergou River valley on the southern slope of Karlik Mountain. (a) Looking southwest from the terminus of No 5Y822C-7 Glacier; (b) Looking northeast on the relict landform of the M_{S5} moraine complex; (c) Looking northwest in the U-shaped valley, about 3 km from the terminus of No 5Y822C-5 Glacier; (d) Looking northeast on the west side of the U-shaped valley, near the M_{S2} moraine complex.

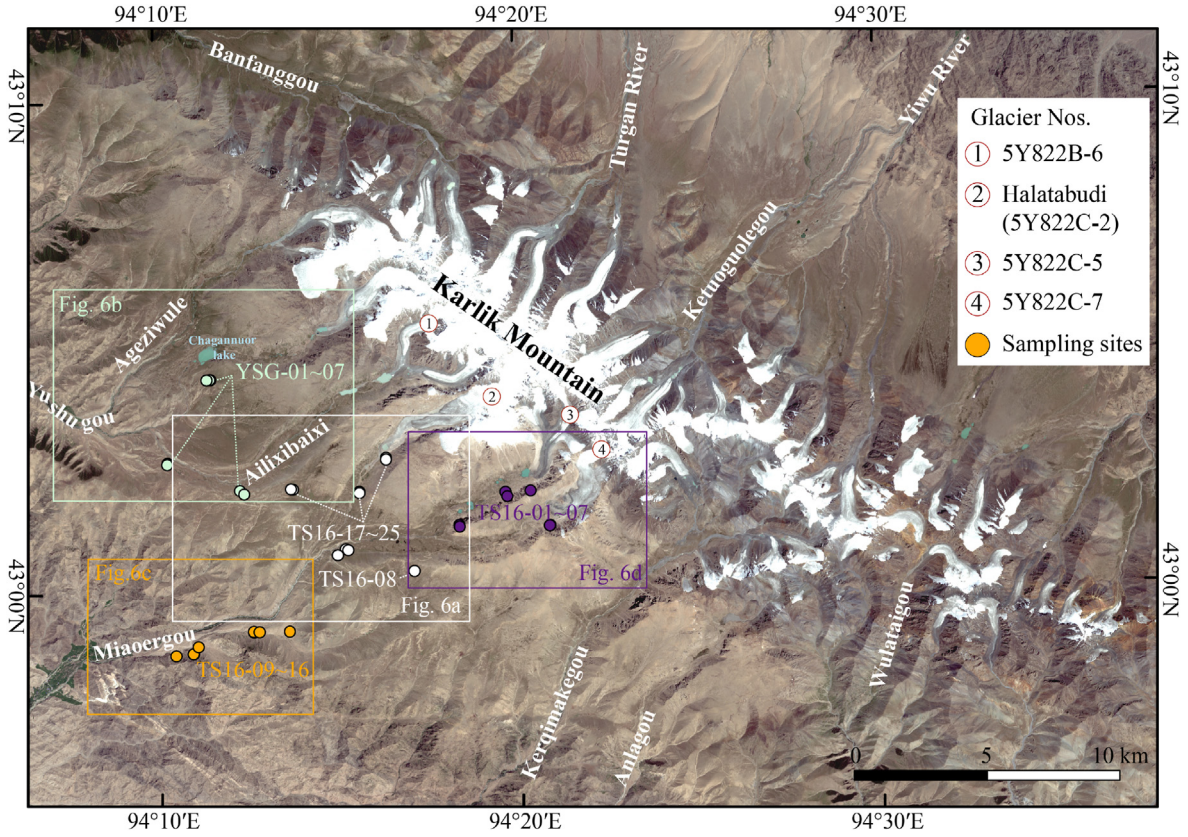

Fig. 3. Modern glaciers, glacial landforms, and ^{10}Be sampling sites (detail in Fig. 6) in the Miaoergou and Yushugou river valleys on the southern slope of Karlik Mountain.

imagery with the data from 1972 (LIGG, 1986), shows that the Halatabudi Glacier in the Miaoergou River valley has retreated about 700 m during the past four decades. Similarly, the terminus of No. 5Y822B-6 glacier in the Yushugou River valley retreated more than 250 m from 1972 to 2011 (Wang et al., 2015). Down valley of these retreating glaciers, there are five sets of moraines and a hummocky moraine preserved along the valley and at the interfluve ridges in these two glaciated valleys (Figs. 2d and 3).

3.2.1. Glacial sequence in the Miaoergou River valley

The first fresh-looking moraine complex (M_{S1}) is 1.5 km down valley from the terminus of the Halatabudi Glacier. This moraine is 150–350 m wide and consists of two end moraines. The sharp-crests of these two end moraines are close to each other and could be classified as a double-crested moraines. A small glacial lake has developed due to the blockage of drainage by this moraine complex. The moraines are about 3–5 m above the lake and 10–15 m above the current stream. Lichen, moss, scattered snow lotus and other pioneer plants are found on this moraine complex, however, no soil or other vegetation has developed. Abundant sub-angular to sub-rounded boulders with diameters 0.5–1 m are present on the moraine, and fresh polished surface or striations could be found on some boulders.

The second set of moraines (M_{S2}) also consists of two end moraines. It is about 0.7 km wide and about 3 km down valley from the terminus of the Halatabudi Glacier, and its crest is about 35–40 m above the stream. A thin soil has developed on the moraine surface, which is mantled by a thick veneer of turf. Boulders with diameters of 1–2 m present on this moraine complex, and the rock varnish and weathering were observed on some boulders.

The third moraine complex (M_{S3}) starts at the confluence of the valleys of the Halatabudi Glacier and glaciers No. 5Y822C-5 and No. 5Y822C-7. Beyond the termini of glaciers No. 5Y822C-5 and No. 5Y822C-7, there are fresh glacial imprints reflecting retreat of the glaciers in recent decades and an M_{S1} moraine complex with sub-angular to sub-rounded boulders without soil or vegetation. No moraine complexes were found corresponding to M_{S2} in these two short glacial troughs but roche moutonnées, glacial rock steps, and large areas of glacially polished surface were present. From the confluence, down the valley to a latero-frontal moraine at 3000 m asl, the M_{S3} moraine complex extends about 6 km along the valley. This moraine complex demonstrates that the ancient glacier was 9.5 km longer than the current Halatabudi Glacier. This moraine has undergone denudation and granitic boulders with diameters of 1–4 m are scattered on the surface, some with very slight granular weathering. A 5–10 cm yellow brown soil has developed on this moraine complex, supporting a vegetation cover of lush grass.

The fourth set of moraines (M_{S4}) is the largest one in this valley. This moraine complex begins at about 3000 m asl and extends about 5 km down the valley and ends at about 2150 m asl. It includes loess sediment about 20–30 cm thick and abundant granitic boulders with diameters of 1–3 m on its surface. The bases of some boulders were buried and exhibit slight granular weathering. Exfoliation and weathering-resistant knobs were observed on some boulders.

The remaining moraine complex (M_{S5}) is only preserved on interfluve ridges. It includes meter-size granitic boulders with slight granular weathering, exfoliation, and weathering-resistant knobs. Some knobs are 3–4 cm higher than the surface and granular weathered debris is scattered around some boulders. Based on the spatial configuration and similarity of weathering features, we hypothesize that the M_{S5} and M_{S4} moraine complexes were formed

during the same glaciation. These two sets of moraines together suggest that a large compound valley glacier or an ice cap has developed in this area during that glaciation.

3.2.2. Glacial sequence in the Yushugou River valley

The glacial sequence in the Yushugou River valley is similar to that in the Miaoergou River valley. Modern glacial landforms that record glacier retreat during the past decades are clearly visible, including a 250 m fresh imprint at the terminus of No. 5Y822B-6 glacier (Wang et al., 2015). An M_{S1} moraine complex occurs about 600–1200 m down valley from the terminus of the modern glacier, and M_{S2} moraine complex occurs about 2.5–4 km down valley from the terminus of modern glacier.

Remnants of an M_{S3}–YSG moraine complex occur on both sides of the Chagannuor stream as continuous lateral moraines, extending from 3380 m asl to 3050 m asl. They are about 4.5 km long and about 50–100 m above the stream. Boulders embedded on the crests are weathered and some also exhibit very slight granular weathering.

Based on the glacial sequence, the landforms to the south side of Ailixibaixi stream should be coeval with M_{S3}. This area consists of undulating relief with alternating convex and concave topography indicative of hummocky moraine. The area of this hummocky moraine is about 3 km^2. It is 40–60 m above the stream, and the height difference between high points and low depressions are 5–7 m. There are abundant slight weathered boulders with diameters of 1–3 m on the surface of the hummocky moraine.

The fourth set of moraines (M_{S4}–YSG) is not as well developed as that in the Miaoergou River valley and is found at the confluence of Ailixibaixi and Ageziwule streams. This moraine complex is partially covered by loess that is about 20–50 cm thick. The moraine includes boulders that exhibit slight granular weathering and a 10–15 cm yellow soil that supports grass and some trees in low areas.

The M_{S5}–YSG moraine is also preserved on interfluve ridges in this valley. Boulders with slight granular weathering are present, and also exhibit exfoliation, weathering-resistant knobs, and granular weathered debris scattered around some large boulders. The distribution and similarity of this moraine complex and M_{S5} in the Miaoergou River valley suggest that they formed during same glacial period. In addition, similar glacial deposits were also found on the interfluve ridges in other adjacent valleys during our fieldwork in 2016. Thus we infer that a large ice cap with many outlet valley glaciers once covered the whole of Karlik Mountain and was developed during the glaciation represented by M_{S4} and M_{S5}.

The lithologies of tills in these two valleys are similar, with the main till clasts being granite, pyroxenite and amphibole plagioclase schist.

4. Methods

4.1. Sampling

Thirty-two samples for ^{10}Be surface exposure dating were collected in the Miaoergou and Yushugou valleys. For the young glacial landforms, granitic or quartz-rich boulders embedded firmly in sharp-crested frontal or lateral moraines with a preserved polished surface were selected. For the older landforms, boulders with rock varnish were sampled. Tall boulders have better-clustered ages than boulders that do not stick out far above a moraine surface (Heyman et al., 2016), so boulders with heights less than 50 cm were avoided during our sampling. Roche moutonnées, rock steps, or bedrock with obvious polished surface were also targeted for sampling.

Boulders with near horizontal or planar top surfaces were sampled, and less than 3 cm of the surface layer was collected using hammer and chisel. To ensure enough pure quartz grains, especially for apparently young glacial landforms, about 1.5 kg of fragments was collected per sample. The sampling site information (latitude, longitude and altitude) were measured using a handheld global positioning system (GPS). The sampled boulders were photographed from different directions (Fig. 4) and their size (length, width and height) were measured (Table 1). Topographic shielding was measured with an inclinometer and compass at 5° intervals. The geomorphic characteristics of the moraines, and the features of glacially polished surfaces were noted and described. In some cases, dip, strike and other features of the samples that could be used to evaluate dating results were also recorded.

4.2. Dating targets preparation

Physical and chemical treatments of the samples were performed at the TCN Preparation Laboratory, State Key Laboratory of Cryospheric Science, Northwest Institute of Eco-Environment and Resources, Chinese Academy of Sciences in Lanzhou, using experimental procedures (Zhao et al., 2021) adapted from Kohl and Nishiizumi (1992) and Dortch et al. (2009). Samples were crushed and 250–500 μm fractions were separated by sieving. These fractions were soaked in H_2O_2 to remove organic matter and in HCl to remove carbonate and other minerals that could be dissolved. Ferromagnetic and mafic minerals and some paramagnetic minerals were separated by Frantz magnetic separator (LB-1) with different currents. After leaching with 5% HF/HNO_3 solution twice and each for about 24 h with heating, the acid-resistant minerals that were heavier or lighter than quartz were removed using silicotungstic acid solution. After this, the residual grains were leached with a low concentration (1–2%) HF/HNO_3 solution for another 2–3 times. The aluminum content of quartz grains was used to evaluate the purity of the samples and was checked by Inductively Coupled Plasma- Optical Emission Spectrometry (ICP-OES).

Quartz grains with aluminum content less than 200 ppm were weighed, and about 0.3 g of ^{9}Be carrier with a concentration of 1017.56 ppm was added before dissolving with concentrated HF solution in Savillex Teflon beaker. A chemical procedural blank was added into each batch (~6 samples). SiF_4 was evaporated off and any trace amount of fluoride was eliminated by fuming with $HClO_4$ three times. The residue was dissolved in dilute HCl, and then run through large anion and cation exchange columns (20 ml) to separate the Be fraction. NH_4OH was added to the Be solution to precipitate $Be(OH)_2$ gel. After the gel was washed three times and transferred to a quartz crucible, the $Be(OH)_2$ was decomposed to BeO in a Muffle furnace at about 950 °C. Finally, the mixture of BeO and niobium powder was pressed into stainless steel cathode.

4.3. AMS measurement and ^{10}Be age calculation

The $^{10}Be/^{9}Be$ ratio for each sample was measured at the Purdue Rare Isotope Measurement Laboratory (PRIME Lab) using AMS, with isotope ratios normalized to standard 07KNSTD (Nishiizumi et al., 2007). The measured $^{10}Be/^{9}Be$ ratios in each batch were corrected using a chemical procedural blank and converted to ^{10}Be concentrations. Topographic shielding was calculated from our field data, and we note that the shielding closely matches that calculated using a Python tool developed by Li (2018) that uses topographic data in an ArcGIS environment. The ^{10}Be ages were calculated for different scaling schemes using the CRONUS Earth version 3.0 online calculator (http://hess.ess.washington.edu/math/v3/v3_age_in.html) (Balco et al., 2008). Quartz weights, ^{9}Be

Fig. 4. Representative photographs of glacially polished surfaces and boulders sampled for ^{10}Be surface exposure age dating.

carrier masses, ^{10}Be/^{9}Be ratios, procedural blank in each batch and related calculation parameters are listed in Table 2. The ages have not be corrected by surface erosion, and correction for snow cover were also omitted because its effect on cosmogenic production in our study area is difficult to evaluate. Therefore, the ages reported here are minimum apparent exposure ages. Ages derived using the LSDn scaling scheme (Lifton et al., 2014b) are reported and discussed in the text. To ensure valid comparisons with previous studies, published ^{10}Be exposure ages in the valleys or regions we compare and discuss in this paper were recalculated using the CRONUS Earth version 3.0 online calculator and the LSDn scaling scheme (supplementary material, SM).

5. Results

In Quaternary glaciation research, samples (boulders, glacially polished surfaces or bedrock) that have experienced prior exposure (nuclide inheritance) or post depositional processes (moraine degradation, boulder toppling, exhumation, shielding, and weathering) before or after they formed will result in overestimated ages or yield underestimated ages (Heyman et al., 2011). Recently, Dortch et al. (2022) proposed using a probabilistic cosmogenic age analysis tool (P-CAAT), which takes these potential effects into account. This method can be used to analyze a glacial landform with three or more ^{10}Be ages. A kernel density estimation (KDE) for the analyzed ages is provided and Gaussian separation of the KDE performed. When performing KDE, the internal uncertainty is applied to analyze the age of each moraine complex, and the external uncertainty is used in regional comparisons. The Gaussian curve contains ^{10}Be ages, the external and internal uncertainties, and the contribution of the internal and external uncertainties to the final age uncertainty. This method includes three available bandwidth estimators (Mean, MADD and STD/IQR). Based on the characteristics of dating results, an appropriate bandwidth estimators is chosen by the users to analyze their ages. Given the potential effects on our ages, we used the P-CAAT method to analyze our dating results and the recalculated TCN ages in the valleys or regions we reference in our discussion (SM).

In the Miaoergou River valley, two samples of the M_{S1} moraine complex were dated to two consistent ^{10}Be ages of 292 ± 30 a (TS16-20) and 272 ± 29 a (TS16-21). Similarly, the M_{S2} moraine complex also had two consistent ^{10}Be ages of 14.2 ± 0.9 ka (TS16-22) and 14.5 ± 0.9 ka (TS16-23). The arithmetic mean values of 282 ± 30 a and 14.3 ± 0.9 ka were used for these two moraine complexes in our discussion. Samples TS16-17 to TS16-19 were derived from the third set of moraines (M_{S3}), and their P-CAAT result is 24.1 ± 4.2 ka (n = 2) (Fig. 5a). The ages of samples TS16-09 to TS16-16, which were collected from the M_{S4} moraine complex were clustered, except for one outlier of 87.1 ± 5.4 ka (TS16-13), and produced a P-CAAT result of 70.1 ± 8.2 ka (n = 7) (Fig. 5b). Three dates of the M_{S5} moraine remnant are 55.3 ± 3.5 ka (TS16-08), 67.5 ± 4.3 ka (TS16-24) and 49.0 ± 3.1 ka (TS16-25), yielding a P-CAAT result of 67.2 ± 9.8 ka (n = 2) (Fig. 5c). Samples TS16-01 to TS16-07 were bedrock samples from roche moutonnées, rock steps and glacially polished surfaces, and the high level of scatter in the dating results (59.7 ± 3.7 ka to 14.6 ± 0.9 ka) suggests that some samples were seriously affected by nuclide inheritance. Whereas, the ages of samples TS16-05 to TS16-07 range from 14.6 ± 0.9 ka to

Table 1
Sampling information for the Miaoergou and Yushugou river valleys on the southern slope of Karlik Mountain, eastern Tianshan range.

Sample ID	Lithology	Latitude (°N)	Longitude (°E)	Elevation (m asl)	Boulder size L/W/H (cm)	Thickness (cm)	Topographic shielding factor
TS16-01	Granite	43.025200	94.345331	3880 ± 3	bedrock	2.0	0.99140
TS16-02	Granite	43.025081	94.345183	3877 ± 4	bedrock	3.5	0.99101
TS16-03	Granite	43.036975	94.336481	3785 ± 3	bedrock	2.0	0.96114
TS16-04	Granite	43.036603	94.324783	3685 ± 3	bedrock	2.0	0.98130
TS16-05	Granite	43.035100	94.325706	3706 ± 3	bedrock	2.0	0.98107
TS16-06	Granite	43.025694	94.303422	3577 ± 3	bedrock	2.0	0.96550
TS16-07	Granite	43.025136	94.303558	3574 ± 3	bedrock	2.0	0.94762
TS16-08	Granite	43.010169	94.282311	3605 ± 3	226 × 198 × 77	2.5	0.99967
TS16-09	Granite	42.982222	94.171739	2367 ± 3	520 × 203 × 200	2.0	0.99462
TS16-10	Granite	42.982894	94.179833	2434 ± 3	230 × 200 × 145	2.0	0.99275
TS16-11	Granite	42.982886	94.179650	2432 ± 3	230 × 205 × 160	2.0	0.99316
TS16-12	Granite	42.985236	94.182097	2457 ± 3	180 × 180 × 170	3.0	0.99447
TS16-13	Granite	42.990197	94.224319	2874 ± 3	320 × 195 × 100	2.0	0.99717
TS16-14	Granite	42.990003	94.207808	2694 ± 3	274 × 110 × 103	3.5	0.99432
TS16-15	Granite	42.990261	94.207681	2693 ± 3	260 × 145 × 80	3.0	0.99400
TS16-16	Granite	42.990089	94.210342	2712 ± 3	265 × 155 × 85	2.0	0.99454
TS16-17	Granite	43.017747	94.250769	3313 ± 3	220 × 200 × 160	2.0	0.99790
TS16-18	Granite	43.017400	94.251839	3314 ± 3	345 × 135 × 155	2.0	0.99745
TS16-19	Granite	43.015728	94.246925	3293 ± 3	390 × 230 × 140	2.0	0.99754
TS16-20	Granite	43.048756	94.269889	3598 ± 3	450 × 300 × 80	3.0	0.96402
TS16-21	Granite	43.048175	94.269967	3602 ± 3	180 × 175 × 100	2.0	0.96905
TS16-22	Granite	43.037267	94.256950	3489 ± 3	210 × 170 × 95	2.0	0.98699
TS16-23	Granite	43.036850	94.256889	3482 ± 3	200 × 130 × 60	2.5	0.98824
TS16-24	Granite	43.038442	94.226739	3541 ± 3	410 × 400 × 140	2.0	0.99960
TS16-25	Granite	43.038564	94.225761	3542 ± 3	500 × 190 × 152	2.0	0.99980
YSG-01	Granite	43.036975	94.204178	3368 ± 3	250 × 230 × 140	2.0	0.99852
YSG-02	Granite	43.038175	94.202294	3369 ± 3	470 × 310 × 150	2.0	0.99938
YSG-03	Granite	43.047242	94.168686	3065 ± 3	230 × 115 × 90	2.0	0.99939
YSG-04	Granite	43.047581	94.168822	3066 ± 3	290 × 154 × 130	2.0	0.99938
YSG-05	Granite	43.075981	94.189081	3376 ± 3	284 × 180 × 125	2.0	0.99829
YSG-06	Granite	43.075897	94.188614	3382 ± 3	240 × 190 × 105	2.0	0.99856
YSG-07	Granite	43.075808	94.187456	3376 ± 3	315 × 310 × 190	2.0	0.99896

18.7 ± 1.2 ka and are consistent with morphological relationships in the valley. In the Yushugou River valley, four samples (YSG-01 to YSG-04) collected from the hummocky moraine has a scatter of dating results, from 11.2 ± 0.9 ka to 17.0 ± 1.2 ka. The dating results on the lateral moraine near Chagannuor Lake are clustered, and their P-CAAT result is 18.1 ± 1.6 ka (n = 2) (Fig. 5d).

Palaeo-ELAs and their depression (ΔELAs) are a very important palaeoclimatic indicators. Here, we used the toe-to-summit altitude method (TSAM) (Benn and Lehmkuhl, 2000 and references therein) that was used in previous studies in this region (Li et al., 2014; Chen et al., 2015) to estimate the palaeo-ELAs and their ΔELAs during different glacial stages in our study (Table 3).

6. Discussion

Glacial landforms in the valleys around Karlik Mountain provide a promising opportunity to understand past glacier fluctuations and to reconstruct palaeoclimate in the eastern Tianshan range. Our ages from the southern slope, combined with previous results from the northern slope (Chen et al., 2015) refine the glacial chronological framework for Karlik Mountain. Assigning ages to glacial landforms can be challenging because of potential problems associated with TCN surface exposure dating. Geomorphic processes experienced by the samples can result in apparent exposure ages that are either too old or too young (Heyman et al., 2011). In this study, the ^{10}Be ages of granitic boulders generally conform to their morphostratigraphical positions, depositional relationship, and weathering conditions, and appear to coincide with the denudation and characteristics of moraines. However, the ages of hummocky moraine, glacially polished surfaces, and bedrock were not well clustered.

Typically, sharp-crested moraines found just beyond modern glacial landforms are presumed to have been deposited during LIA glacial advances (Grove, 2004; Shi et al., 2006, 2011). Two consistent ^{10}Be ages for M_{S1} moraine samples of 292 ± 30 a (TS16-20) and 272 ± 29 a (TS16-21) confirm that this moraine complex was deposited during the LIA (Fig. 6a). Scattered ^{10}Be ages of the first moraine complex (M1) in the Turgan River valley on the northern slope have been interpreted as the impact of nuclide inheritance, but after removing obvious outliers (Chen et al., 2015), the P-CAAT result of the remaining ages is 831 ± 525 a (n = 6), beyond the scope of the LIA defined by the IPCC (2013) and does not overlap with the M_{S1} moraine ages. It seems that glaciers on the southern and northern slopes of Karlik Mountain were responding differently to regional climate change. Future work should consider what conditions might lead glaciers on the northern slope to expand and begin retreating several centuries earlier than the LIA maximum observed on the southern slope.

As part of dating LIA glacial landforms around the world (Solomina et al., 2016 and references therein), LIA landforms across the Tianshan range have been investigated by lichenometry, AMS^{14}C and ^{10}Be dating techniques. At the headwater of the Urumqi River, the first set of moraines has been extensively investigated since 1980s. It has been dated by lichenometry (Chen, 1989), and AMS^{14}C dating techniques (Yi et al., 2004). In the past decade, this moraine complex was dated using ^{10}Be exposure dating techniques (SM), the outmost end moraine yields age of 445 ± 72 a (n = 4) (Li et al., 2014) and the second one was dated to 292 ± 86 a (n = 4) (Li et al., 2016b). In addition, LIA glacial landforms at the Haxilegen Pass were dated to 300 ± 56 a (n = 3) (HDBA inner), 527 ± 816 a (n = 4) (HDBA outer) and 321 ± 66 a (n = 4) (HDBB) (Li et al., 2016b), and the TK1 and SR1 moraine complexes in the Takelekete and Sairenwususala valleys on Nalati Mountain were dated to 332 ± 146 a (n = 3) and 336 ± 195 a (n = 3) (Zhang et al., 2016a). In the west segment of the Tianshan range, two individual ^{10}Be ages of the moraine complex IV and V in the Ala Archa valley in

Table 2
^{10}Be apparent exposure ages calculated using the CRONUS online calculator and the related calculation parameters.

Sample ID[a]	Quartz (g)	^{9}Be carrier (g)	^{10}Be/^{9}Be (10^{-15})	^{10}Be concentration (10^{4} atoms/g)	St			Lm			LSDn		
					Age (years)	Internal error (years)	Extra error (years)	Age (years)	Internal error (years)	Extra error (years)	Age (years)	Internal error (years)	Extra error (years)
TS16-01	70.0707	0.3022	13814.80 ± 210.78	405.0638 ± 7.3906	70,387	1307	5809	66,172	1228	5193	59,665	1105	3740
TS16-02	70.4387	0.3000	10748.50 ± 140.17	311.2135 ± 5.1154	54,654	911	4471	51,674	860	4019	45,100	750	2794
TS16-03	50.7317	0.3097	3758.99 ± 57.43	155.9467 ± 2.8492	29,094	535	2376	27,599	508	2145	24,975	459	1552
TS16-04	70.3442	0.2988	4664.24 ± 85.67	134.6533 ± 2.8174	25,959	547	2135	24,785	522	1942	22,649	477	1426
TS16-05	70.1882	0.3073	2803.07 ± 44.25	83.3852 ± 1.5595	15,857	298	1292	15,724	295	1220	14,582	274	906
TS16-06	70.2626	0.2999	3072.15 ± 42.78	89.0990 ± 1.5286	18,496	319	1502	18,172	313	1404	16,863	291	1041
TS16-Blk 1		0.3040	2.17 ± 0.45	4.4856 ± 0.9302									
TS16-07	70.1088	0.3008	3344.36 ± 70.21	97.9602 ± 2.2796	20,764	486	1719	20,220	473	1596	18,728	438	1193
TS16-08	70.1986	0.3033	10978.30 ± 221.12	318.9577 ± 7.1739	63,970	1462	5339	60,753	1387	4830	55,303	1261	3541
TS16-09	70.4362	0.3027	6235.59 ± 118.20	186.3668 ± 3.9956	79,537	1740	6642	75,242	1644	5981	73,132	1597	4676
TS16-10	70.6898	0.3017	5565.21 ± 100.93	159.8924 ± 3.3128	65,183	1373	5411	62,020	1305	4901	60,335	1269	3830
TS16-11	70.1432	0.3002	5558.17 ± 100.92	165.5143 ± 3.4323	67,575	1425	5614	64,076	1350	5067	62,330	1313	3959
TS16-12	70.1755	0.3137	5848.46 ± 103.96	169.8884 ± 3.4663	68,732	1427	5705	65,054	1349	5139	63,192	1310	4008
TS16- Blk2		0.3014	2.12 ± 1.08	4.3448 ± 2.2134									
TS16-13	60.1108	0.3020	9277.41 ± 61.02	316.8979 ± 3.7936	98,057	1203	8030	92,140	1129	7162	87,088	1066	5359
TS16-14	60.4102	0.3016	5684.05 ± 63.34	192.9233 ± 2.8893	67,294	1025	5503	63,770	970	4956	61,265	932	3787
TS16-15	60.0849	0.2999	6620.99 ± 47.16	224.6731 ± 2.7590	78,332	981	6387	74,034	926	5732	70,545	882	4327
TS16-16	60.1602	0.3123	6184.91 ± 51.88	218.2786 ± 2.8497	74,461	990	6075	70,281	934	5445	66,977	889	4116
TS16-17	60.4129	0.2992	2257.04 ± 23.80	75.9710 ± 1.1050	17,718	259	1430	17,459	255	1340	16,435	240	1003
TS16-18	60.9844	0.3066	3389.53 ± 29.48	115.8361 ± 1.5360	27,075	361	2184	25,803	344	1978	24,033	321	1462
TS16-Blk3		0.2981	1.11 ± 0.95	2.2500 ± 1.9256									
TS16-19	36.5463	0.2999	2059.91 ± 32.51	114.8486 ± 2.1476	27,171	512	2221	25,891	487	2014	24,138	454	1503
TS16-20	36.8888	0.3016	20.10 ± 1.54	1.0270 ± 0.0881	212	18	25	273	23	31	292	25	30
TS16-21	36.7376	0.3029	18.87 ± 1.51	0.9671 ± 0.0871	196	18	24	253	23	30	272	24	29
TS16-22	36.6686	0.2975	1296.72 ± 20.84	71.4459 ± 1.3542	15,223	290	1241	15,141	288	1176	14,208	270	884
TS16-23	36.9892	0.3068	1285.48 ± 20.20	72.4094 ± 1.3505	15,536	291	1266	15,427	289	1197	14,481	271	899
TS16-24	36.8793	0.2998	6897.27 ± 133.78	381.1646 ± 8.3198	79,137	1762	6616	74,542	1658	5932	67,540	1499	4321
TS16-Blk4		0.3028	1.62 ± 0.31	3.3355 ± 0.6382									
TS16-25	40.1283	0.3018	5433.56 ± 96.10	277.6760 ± 5.6460	57,295	1182	4741	54,527	1124	4295	48,970	1008	3094
KL2013-Blk 1		0.2989	3.84 ± 1.16	7.8045 ± 2.3576									
YSG-01	31.3673	0.3060	1198.83 ± 15.56	77.7579 ± 1.2874	17,550	292	1423	17,304	288	1335	16,251	270	1000
KLGX-Blk2		0.3065	3.77 ± 1.86	12.3127 ± 4.1885									
YSG-02	31.1561	0.3062	752.98 ± 37.53	50.1906 ± 2.5582	11,294	577	1065	11,621	594	1057	11,164	571	873
YSG-03	30.0791	0.3069	970.50 ± 38.27	67.1980 ± 2.7393	18,088	741	1615	17,805	729	1527	16,973	695	1222
YSG-04	14.6358	0.3061	363.82 ± 8.46	51.4656 ± 1.3114	13,831	354	1152	13,875	355	1103	13,366	342	862
YSG-05	29.6016	0.3057	1292.63 ± 21.09	90.6349 ± 1.7373	20,361	392	1664	19,864	383	1545	18,587	358	1158
YSG-06	20.6049	0.3061	962.88 ± 16.01	97.0699 ± 1.8878	21,733	425	1778	21,080	412	1642	19,701	385	1230
YSG-07	29.2102	0.3046	1217.92 ± 20.81	86.2209 ± 1.7100	19,351	386	1584	18,957	378	1478	17,745	354	1109
YSG-Blk 1		0.3072	1.92 ± 0.48	4.0106 ± 1.0027									

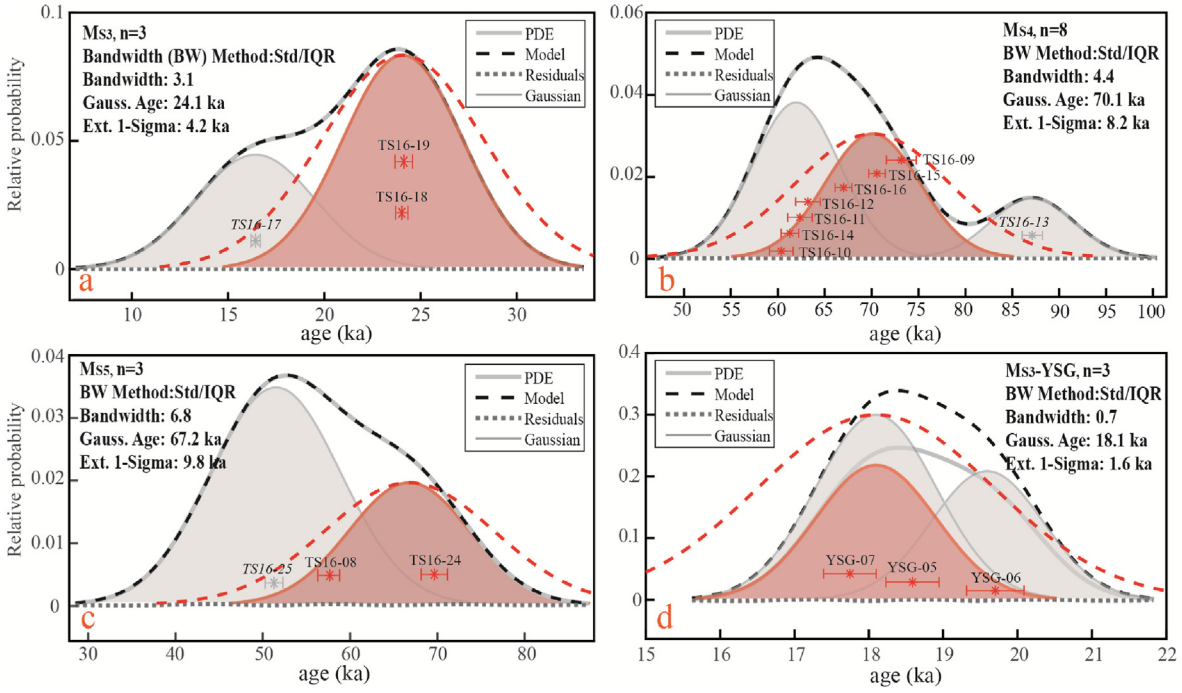

Fig. 5. Dating results were analyzed using the P-CAAT (Dortch et al., 2022). The sample No. s in gray italics are outliers or excluded by this method.

Table 3
Palaeo-ELAs (m asl) and ΔELAs (meters) for selected glacial stages on the southern and northern slopes of Karlik Mountain (reconstructed by TSAM).

Glacial stages	Modern ELA	LIA		Lateglacial		LGM_G		MIS 3		MIS 4	
		Palaeo-ELA	ΔELA	Palaeo-ELA	ΔELA	Palaeo-ELA	ΔELA	Palaeo-ELA	ΔELA	Palaeo-ELA	ΔELA
Southern slope	4284	4203	81	4143	141	3778	506	/	/	3573	711
Northern slope	4256	4198	58	4078	178	/	/	3652	604	3630	626

the Kyrgyz Front Mountain are 346 ± 89 a and 677 ± 115 a (Koppes et al., 2008), in the Barskoon Valley and on the southern slope of Zalisky Ala Tau Mountain, the innermost moraines were dated to 449 ± 259 a (n = 3) and 325 ± 5 a (n = 3), respectively (Batbaatar et al., 2020). Most of these ages correspond to the regional glacial stages SWHTS 1 A in the semi-arid western end of the Himalayan-Tibetan orogen (Dortch et al., 2013) and MOHITS 1 A in the monsoon-influenced Himalaya-Tibetan area (Murari et al., 2014).

Glaciers typically advance in colder and/or wetter climate periods. LIA climate has been reconstructed from a range of climate archives. High-frequency cold climate variations have been reconstructed from records of multiple proxies in the Northern Hemisphere, the Tibetan Plateau (TP) and its surroundings (Moberg et al., 2005; Thompson et al., 2006; Mischke and Zhang, 2010). An analysis of effective moisture conditions indicate that the areas dominated by the Asian monsoons had lower effective moisture since 3 ka BP, while in the Westerlies-dominated areas no such uniform decline has been observed (Herzschuh, 2006). A study of sediment cores retrieved from Bosten Lake revealed a humid climate from 1500 AD to1900 AD (Chen et al., 2006). Later, an integrated analysis of multiple proxies, including ice cores, tree rings, lacustrine sediments, historical documents, glacial fluctuations and archeological data has revealed that the climate during the LIA in Central Asia was cold and humid (Yang et al., 2009). Therefore, the LIA glacial advance in the Tianshan range is likely due to period of cold and wet climate.

The pattern of moraines in the TP and its surroundings suggest that multiple glacial advances occurred in the Holocene prior to the LIA (Shi et al., 2006, 2011; Dortch et al., 2013; Murari et al., 2014; Owen and Dortch, 2014). However, in our research area no landforms corresponding to these glacial advances have been observed, and no moraine ages record Holocene glacial events, except for the LIA event. This suggests that any Holocene advances here were less extensive than the LIA advance.

Two consistent M_{S2} ^{10}Be ages (TS16-22: 14.2 ± 0.9 ka, and TS16-23: 14.5 ± 0.9 ka) have been reported in our study area (Fig. 6a). Combing this with the P-CAAT ^{10}Be age (14.0 ± 1.1 ka, n = 2) of the M3 moraine complex in the Turgan River valley (Chen et al., 2015), we concluded that the M_{S2} moraine complex was deposited during the Lateglacial. Evidence of a Lateglacial event have been identified and dated by TCNs in several areas across the Tianshan range (SM) including a moraine and its three clustered ^{10}Be ages (13.2 ± 1.6 ka, n = 3) in the Koksu Valley of the Alay Mountain (Abramowski et al., 2006), a latero-frontal moraine (M2, 15.2 ± 1.8 ka, n = 3) in the Kitschi-Kurumdu Valley in the At Bashi Mountains (Zech, 2012), a lateral moraine (14.4 ± 0.7 ka, n = 4) along the north side of Inylchek River valley (Lifton et al., 2014a), a distinct marginal moraine ridge (BOR2, 14.4 ± 1.5 ka, n = 2) in the Bordoo Valley and a terminal moraine (KOY1, 15.9 ± 1.8 ka, n = 3) in the Koyandy Valley (Blomdin et al., 2016). In Batbaatar et al.'s (2020) summary of Central Asian studies, Lateglacial event were identified in several sites, including the moraines at the mouth of the Muzart River, in the Barskoon Valley, in the Gulbel Valley, and on the southern slope of the Zalisky Ala Tau Mountain. In addition, ^{10}Be ages ranging from 16 to 19 ka at the headwater of the Urumqi River valley (Kong et al., 2009; Li et al., 2011) imply that glacier fluctuations occurred there

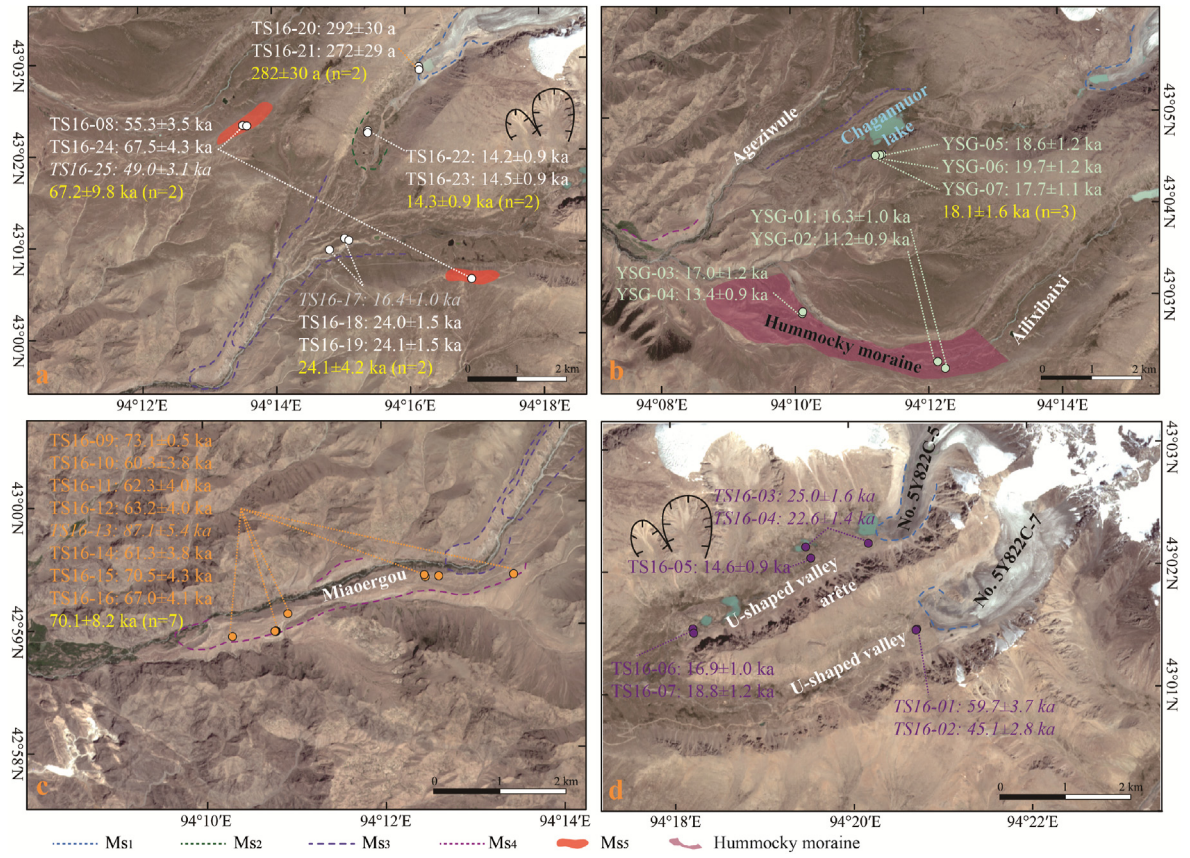

Fig. 6. Moraine complexes and their ^{10}Be ages on the southern slope of Karlik Mountain, the sample No. s in gray italics are outliers or are not consistent with the geomorphological relationship.

during this period. More work should be done in the future to determine whether these landforms were formed by glacial advance or standstills during the last deglaciation.

The ages for samples from the M_{S3} moraine complex in the Miaoergou River valley and the lateral moraines on both sides of the Chagannuor stream in the Yushugou River valley are 24.1 ± 4.2 ka (n = 2) and 18.1 ± 1.6 ka (n = 3) respectively (Fig. 6a and b). These dates are within the chronozone level 1 (19–23 cal ka) or level 2 (18–24 cal ka) of the LGM_G that suggested by the EPILOG research group (Mix et al., 2001), and also within the LGM_G time-frame (~19–26.5 ka) defined by Clark et al. (2009) based on the timing of the maximum extents of ice sheets and mountain glaciers around the globe. Our findings confirm that glacial landforms of the LGM_G are preserved on Karlik Mountain. The M4 moraine complex in the Turgan River valley may have been formed during the LGM_G, as suggested by Chen et al. (2015), unfortunately no numeric ages were obtained to constrain it. Ages of glacial landforms coeval with the LGM_G have been dated by different numerical dating techniques and reported across the Tianshan range (Yi et al., 2004; Abramowski et al., 2006; Zhao et al., 2009, 2010, 2012, 2015; Narama et al., 2007, 2009; Koppes et al., 2008; Li et al., 2014; Zech, 2012; Lifton et al., 2014a; Blomdin et al., 2016; Batbaatar et al., 2020). Among these studies, the P-CAAT results of recalculated ^{10}Be ages (SM) indicate that a glacial event during the LGM_G can be confirmed throughout this range (Fig. 1). The AK3 lateral moraines in the Aksu Valley in the Turkestan Mountain date to 26.3 ± 4.9 ka (n = 4) (Abramowski et al., 2006). The M3 moraine complex is 20.0 ± 2.0 ka (n = 5) in the Kitschi-Kurumdu Valley (Zech, 2012). At the Tumur Peak area, the innermost terminal moraine is 22.2 ± 2.4 ka (n = 4) at the junction of the Inylchek and Sary-Dzaz rivers, hummocky moraine is 21.9 ± 2.3 ka (n = 2) in the Sary Dzaz Valley (Lifton et al., 2014a). The moraine BOR3 is 23.3 ± 3.8 ka (n = 3) in the Bordoo Valley (Blomdin et al., 2016). The M3 moraine complex is 23.9 ± 1.6 ka (n = 4) in the Ala River valley (Li et al., 2014), and the ages of M1 and M2 moraine complexes also indicate that they were formed by glacier fluctuations during the LGM_G. Batbaatar et al.'s (2020) dating results indicate that LGM_G moraine complexes were preserved in several valleys, such as in the Suek, Muzart and Gulbel Valleys, and on the southern slope of Zalisky Ala Tau Mountain.

Four samples derived from the hummocky moraine in the Yushugou River valley were dated to 16.3 ± 1.0 ka (YSG-01), 11.2 ± 0.9 ka (YSG-02), 17.0 ± 1.2 ka (YSG-03) and 13.4 ± 0.9 ka (YSG-04) (Fig. 6b). The scattered ages make it difficult to assign a specific glacial event to this landform, although the glacial sequence, morphological relationship, characteristics of moraine, weathering degree of boulders and other features suggest that the hummocky moraine is coeval with LGM_G. Our scattered ^{10}Be ages are similar to those of some previous studies (Zech et al., 2005; Reuther et al., 2011; Zech, 2012, 2012iner et al., 2015). The discrepancy between dating results and the actual ages of these landforms likely reflects post-depositional processes. A study in the Pamir Mountains by Zech et al. (2005) suggested that an extend period of melt by buried glacier ice produces long-lived surface instability for hummocky moraine. A similar explanation was given for the scattered ages of a large piedmont lobe glacier in southeast Germany (Reuther et al., 2011), hummocky moraines in the Kitschi-Kurumdu Valley, Tianshan range (Zech, 2012), and in the Central Taurus Mountains, southern Turkey (Çiner et al., 2015). In this study, if the oldest age of YSG-03 (17.0 ± 1.2 ka) and the youngest

age of YSG-02 (11.2 ± 0.9 ka) are assumed to the beginning and end formation time of this hummocky moraine, it means that surface instability lasted at least 6–7 ka.

Considering both morphological relationships and the ages of M_{S2} and M_{S3}, the ages of glacially polished surfaces and bedrock in our study should be coeval with either Lateglacial or post-LGM_G. However, the dating results for samples TS16-01 to TS16-07 range from 14.6 ± 0.9 ka to 59.7 ± 3.7 ka (Fig. 6d). Previous studies have noted that the ages or nuclide concentrations for glacially polished surfaces are sometimes greater than those of nearby glacially transported boulders (Briner and Swanson, 1998; Bierman et al., 1999), and in other cases dating results (nuclide inventories) for glacially polished surfaces are consistent with the deglaciation age of the surface (Nishiizumi et al., 1989; Clark et al., 1995; Kelly et al., 2006; Zhang et al., 2016b). These studies demonstrate that subglacial erosion by abrasion is sometimes insufficient to remove cosmogenic nuclide inventories that have been accumulated during ice-free periods. In some cases, it is possible to use differences in ages to infer depths of glacial erosion, for example, patterns of subglacial erosion in different parts of the cross section of glacial U-shaped valleys have different erosion (Fabel et al., 2002, 2004; Li et al., 2005), or across roche moutonnées. Our field observations and photos demonstrate that samples TS16-01 and TS16-02 were collected from high points of bedrock in the trough, whereas samples TS16-03 and TS16-07 collected from the bottom (Fig. 6d). Samples TS16-01 to TS16-04 were taken on surfaces without glacial polish, whereas obvious polished surfaces were observed on samples TS16-05 to TS16-07. Based on the glacial sequence, morphological relationships and observations of glacial polish, the ages of samples TS16-01 to TS16-04 (22.6 ± 1.4 ka to 59.7 ± 3.7 ka) appear to be overestimated, whereas the ages of samples TS16-05 to TS12-07 (14.6 ± 0.9 ka to 18.7 ± 1.2 ka) are consistent with the morphological relationships (Fig. 6d). This suggests that erosion at sampling sites of TS16-01 to TS16-04 was insufficient to remove inheritance (<2 m), whereas erosion at sampling sites of TS16-05 to TS16-07 was >2 m. Our findings, together with previous studies have shown that there is not yet an obvious way to determine in advance of sampling whether a glacially polished surface or bedrock has been fully reset by subglacial erosion, so a cautious approach to sample site selection, sampling strategy, and interpretation of results is needed.

The ages of samples TS16-09 to TS16-16 from M_{S4} moraine complex, range from 60.3 ± 3.8 ka to 87.1 ± 5.4 ka. After removing the outlier of 87.1 ± 5.4 ka (TS16-13), the rest of the ages are clustered and their P-CAAT result is 70.1 ± 8.2 ka (n = 7) (Fig. 6c), indicating that this moraine complex was formed in the early part of last glaciation, corresponding to MIS 4. Based on the glacial sequence and morphological relationship, two older ^{10}Be ages (YW-09-11-2: 57.9 ± 3.7 ka and YW-09-11-3: 75.7 ± 5.6 ka) were assigned to the M6 moraine complex in the Turgan River valley by Chen et al. (2015), and it was tentatively concluded that the M6 moraine was deposited during MIS 4 or an older glaciation. In combination, these suggest that the largest local last glacial maximum (LGM_L) occurred during MIS 4 rather than the LGM_G of MIS 2. Three samples of the M_{S5} moraine complex were dated to 55.3 ± 3.5 ka (TS16-08), 67.5 ± 4.3 ka (TS16-24) and 49.0 ± 3.1 ka (TS16-25), and their P-CAAT result is 67.2 ± 9.8 ka (n = 2) (Fig. 6a). Evidence of weathering on these boulders, such as protubing knobs and granular weathered debris around boulders, indicate that their real ages should be older. Based on the morphological relationship, preservation conditions and minimum ages, we conclude that both the M_{S4} and M_{S5} moraine complexes were formed during the same glaciation. The distribution of these two moraine complexes and other similar glacial deposits on the interfluve ridges in other adjacent valleys suggest that a large ice cap with many outlet valley glaciers once covered Karlik Mountain during the early part of the last glaciation.

An MIS 4 glaciation has been identified and dated in many valleys across the Tianshan range (Abramowski et al., 2006; Narama et al., 2007, 2009; Koppes et al., 2008; Zhao et al., 2009, 2010, 2012; Zech, 2012; Li et al., 2014; Lifton et al., 2014a; Blomdin et al., 2016; Zhang et al., 2016a; Batbaatar et al., 2020). As pointed out by Owen and Dortch (2014), there is a glaciation peak at 60–75 ka in the Pamir Plateau and Tianshan range, our dates and the recalculated ^{10}Be ages (SM) that were not included in their study confirm this result. Examples of MIS 4 glaciation include the M5 moraine complex in the Ala Valley of the Tianger Mountains (Li et al., 2014), and TK5 and AK5 moraine complexes in the Takelekete and Aiken valleys in the Nalati Mountains (Zhang et al., 2016a). In the west segment of this range, examples of MIS 4 glaciation include the lowermost terminal moraine (KK) at the valley entrance near Daraut Kurgan in the Koksu Valley in the Alay Mountains (Abramowski et al., 2006), M6 moraine complex (hummocky moraine) in the Kitschi-Kurumdu Valley in the At Bashi Mountains (Zech, 2012), moraine remnant at somewhat higher elevation in the Inylchek Valley on the western slope of Tumur Peak (Lifton et al., 2014a), and moraines in the Alashanje Valley (Batbaatar et al., 2020).

Five OSL ages for the M5 moraine complex in the Turgan River valley on the northern slope range from 37.4 ± 4.0 to 44.2 ± 4.3 ka (Chen et al., 2015), and four clustered dates indicate that this set of moraines were deposited in the mid-MIS 3. Glacial advance during MIS 3 has been reported across the TP and its surroundings, especially in monsoon-influenced areas (Owen and Dortch, 2014). Likewise, TCNs, OSL and ESR dating results of this glaciation across the Tianshan range have been reported (Zhao et al., 2006, 2009, 2010; Koppes et al., 2008; Narama et al., 2009; Li et al., 2014; Lifton et al., 2014a; Zhang et al., 2016a; Batbaatar et al., 2020). MIS 3 is a relative warm period in the last glacial cycle, so more cautious explanation should be given to this plausible glacial advance.

Given the chronology of the moraine complexes in study area, there is considerable interest in considering underlying climate forcing mechanisms that drive these glacial advances. δ^{18}O records from marine sediments have been used as a proxy for global climate change and ice volumes (Lisiecki and Raymo, 2005), and δ^{18}O records from the Guliya ice core, from the West Kunlun, can serve as a local temperature indicator for the TP and its surroundings (Thompson et al., 1997), especially for the northwestern part of High Mountain Asia. The formation time of the moraine complexes in our study area are in phase with the negative δ^{18}O excursion and low δ^{18}O trough that are present in the record of the Guliya ice core during MIS 2 and 4 (Thompson et al., 1997), and correspond with peaks in global ice volume during the last glacial cycle (Lisiecki and Raymo, 2005) and the low insolation record at 65° in the Northern Hemisphere (Berger and Loutre, 1991) (Fig. 7). They also correspond with the speleothem record in East Asia Monsoon area (Wang et al., 2008). Thus, geological evidence for MIS 4 and 2 glacial advances correlates well with records of global temperature that show cold periods during these times. A comprehensive review by Doughty et al. (2021) has pointed out that many glacier systems of different sizes world-wide, as well as portions of some ice sheets, were more extensive during MIS 4 and MIS 3 than they were during MIS 2. Karlik Mountain is another good example of this pattern.

Precipitation in Central Asia is largely associated with the westerlies, therefore, the North Atlantic and some inland lakes, such as the Black Sea, the Caspian Sea and the Aral Sea are the main moisture source for glaciers in the Tianshan range (Benn and Owen, 1998). Spatiotemporal variations in precipitation in Central Asia during the last glacial cycle were impacted by the growth and decay

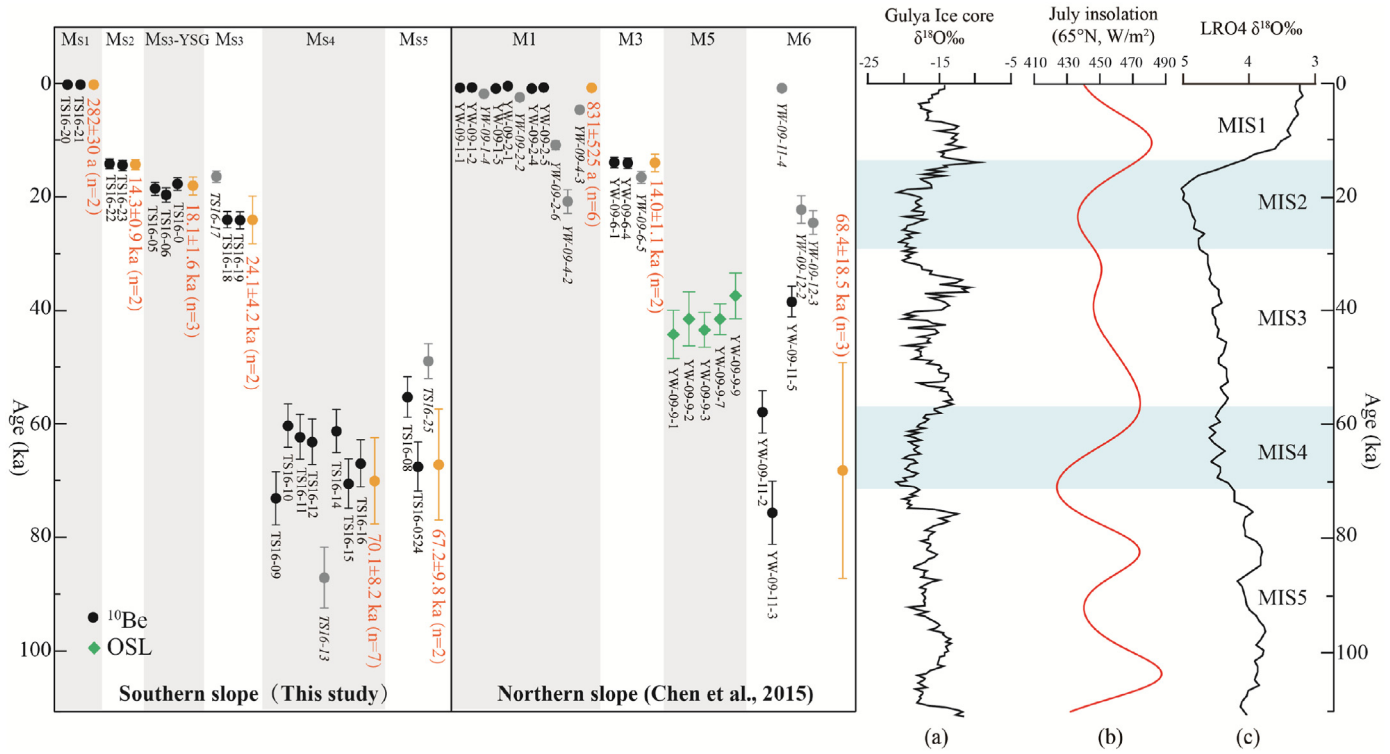

Fig. 7. A comparison of dating results from Karlik Mountain with other climatic proxies: a, $\delta^{18}O$ records of the Guliya ice core (Thompson et al., 1997); b, July insolation at 65°N (Berger and Loutre, 1991); c, $\delta^{18}O$ records for LR04 and Marine Oxygen Isotope Stage (MIS) (Lisiecki and Raymo, 2005).

of ice sheets in northwest Europe. This was, because of changes in atmospheric circulation associated with the presence of the ice sheet, and changes in oceanic circulation associated with changing sea level, salinity, and sea surface temperature. The Eurasian ice sheet complex (EISC), which included the Celtic, Fennoscandian, and Barents (and Kara) Sea Ice Sheets, reached its greatest extent and volume at 22.7 ka BP (Patton et al., 2016), and had relatively minor fluctuations in volume and extent during c. 23.0–19.5 ka BP (Patton et al., 2017). Changes in the extent of glaciers across the Tianshan range are out of phase with the EISC, as glacial advances in the Tianshan became smaller from MIS 4 to MIS 2. This difference has been linked to arid conditions in Central Asia during the last glacial cycle, especially during the LGM_G (Shi et al., 2000). As the separate, independent ice sheets grew from MIS 4 to a large EISC in MIS 2, this created an orographic barrier that reduced the amount of moisture carried by the westerlies to Central Asia. In other words, during MIS 4 the orographic barrier effect was small, and a relatively humid climate resulted in more extensive glacial advances than occurred during LGM_G when the orographic barrier effect was larger. An extreme dry condition occurred in Central Asia around 21 ka (Herzschuh, 2006), thus, a cold and dry climate restricted the development of palaeoglaciers during the LGM_G in our study area.

Based on OSL ages, Chen et al. (2015) suggested that the M5 moraine complex in the Turgan River valley was formed by a MIS 3 glacial advance. This was a relative warm period in the last glacial cycle, however, some previous studies have argued that, in monsoon-influenced areas, increased solar radiation strengthened the Indian Summer Monsoon bringing in more precipitation that drove glacial advance at high elevations despite increases in melting due to warming (Owen and Dortch, 2014 and references therein). Based on $\delta^{18}O$ records of the Guliya ice core and other climatic proxies in the TP and its surroundings, mid-MIS 3 was a relatively cold and wet period (Shi and Yao, 2002), and proxies for effective moisture indicate that a moderately wet climate occurred during this sub-stage (Herzschuh, 2006), and thus this was a favorable climate for developing glaciers in the TP and its surroundings (Zhao et al., 2007; Wang, 2010). An alternative interpretation is that these moraine ages reflect exhumation during a MIS 3 intensive denudation period, and thus the exhumed boulders' ages are younger than their "real ages" (Schaefer et al., 2008). Chen et al. (2015) argued that their OSL samples would not have been affected by surface denudation, and thus reflect the formation age of the M5 moraine complex, however in some cases partial bleaching complicates the interpretation of OSL results for glacial deposits (Fuchs and Owen, 2008; Ou et al., 2015; Gribenski et al., 2018). Challenges with ESR ages have also been noted in some studies (Kong et al., 2009; Li et al., 2011; Blomdin et al., 2016), and more generally careful evaluation of OSL, ESR, and TCN ages is needed to assign ages for glacial deposits prior to MIS 2 in the Tianshan range (Blomdin et al., 2016), especially when small sample size and/or poor resolution hinders the development of reliable chronological frameworks. Finally, we note that climate-glaciation simulations did not indicate widespread glacier advances in the Tianshan range during MIS 3 (Yan et al., 2023).

In Quaternary glaciation research, palaeo-ELAs and their changes (ΔELAs) can be used to assess the significance of spatio-temporal variations of past glaciers. In our study, the reconstructed ELAs of LIA, Lateglacial, LGM_G and MIS 4 glaciation were 4203 m, 4143 m, 3778 m and 3573 m, respectively, and ΔELAs were 81 m, 141 m, 506 m and 711 m respectively. Modern and ancient ELAs on the southern slope are higher than those on the northern slope (Fig. 8, Table 3), likely because glaciers on south-facing slopes in the Northern Hemisphere receive more solar radiation. However, ΔELAs are small on both north- and south-facing slopes during LIA and Lateglacial. The palaeo-ELA and ΔELA during MIS 4 in this study is complicated by the fact that we infer that a large ice cap covered

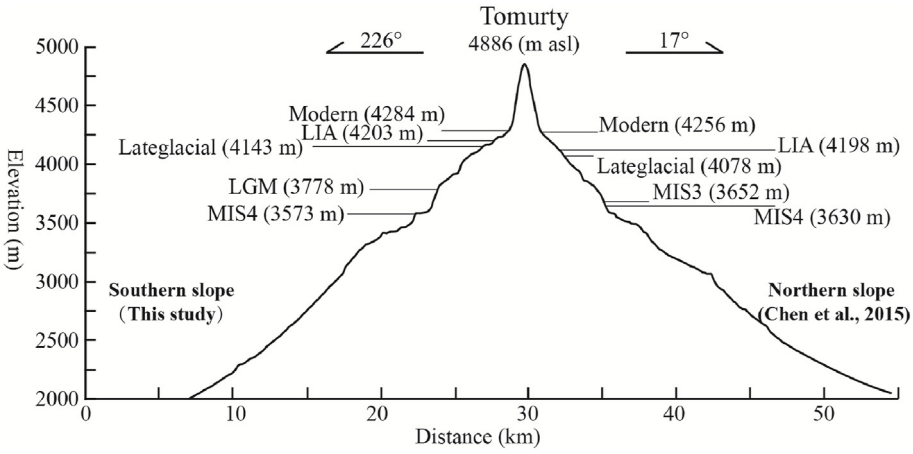

Fig. 8. A comparison of reconstructed palaeo-ELAs for different glacial stages on southern and northern slopes of Karlik Mountain.

the whole of Karlik Mountain during that period, and the ELA of a compound valley glacier is different to that of an ice cap. In combination with previous studies (Li et al., 2014; Chen et al., 2015), there is currently no obvious pattern of ΔELAs from north to south or from west to east during different glacial stages in this region. Hopefully, further robust glacial chronologies and reconstructed ΔELAs will provide more complete insight into the pattern of ΔELA for the Tianshan range.

7. Conclusion

New ^{10}Be surface exposure ages of moraine complexes in the Miaoergou and Yushugou river valleys on the southern slope of Karlik Mountain, combined with previously published ^{10}Be and OSL ages in the Turgan River valley on the northern slope, identify five glacial events in the easternmost part of the Tianshan range, corresponding to the LIA, Lateglacial, LGM_G, mid-MIS 3 and MIS 4. The landforms of M_{S4} and M_{S5} indicate that the largest local ice extent, LGM_L, occurred during MIS 4, rather than the LGM_G of MIS 2, and that a large ice cap with many outlet valley glaciers developed and covered Karlik Mountain during MIS 4 glaciation. The landforms and their ages show that glacial advances in this area have been less extensive since MIS 4. These results are consistent with most other parts of the Tianshan range, suggesting similar climate controls on the timing of Quaternary glaciations along the whole range. These changes have been linked to the impact of the EISC on the supply of moisture to Central Asia from the westerlies. The only Holocene glacial advance recorded by the glacial landforms on Karlik Mountain is the LIA, indicating that any earlier Holocene advances were less extensive than the LIA advance.

Dating formation ages of glacial landforms with TCNs includes several challenges. In this study, scattered ^{10}Be ages from boulders taken on hummocky moraine indicate that this moraine experienced surface instability for several thousand years. The scatter of ages on glacially polished surfaces and bedrock indicate that inheritance may be present in some samples, reaffirming the importance of a cautious sampling strategy and the use of multiple isotopes for glacially polished surfaces or bedrock. In addition, a cautious approach to geomorphological discrimination, sample site selection, and interpretation of results are also very important.

Credit author statement

JZ designed and conducted the fieldwork, experiments; JZ, JH and MC were involved ^{10}Be data production and interpretation; JQ, HJ, WG and HZ conducted the fieldwork, experiments and prepared figures. All authors contributed to writing, reviewing, and editing the paper.

Declaration of competing interest

The authors declare that they have no known competing financial interests or personal relationships that could have appeared to influence the work reported in this paper.

Data availability

Data will be made available on request.

Acknowledgements

We thank Limin Zheng and Yuming Lu for their fieldwork assistance. Thomas E. Woodruff for helping measure the ^{10}Be dating targets in the PRIME Laboratory, Purdue University. This work was supported by the National Natural Science Foundation of China (Nos. 41771018, 41830644, 41371028), the Second Tibetan Plateau Scientific Expedition and Research Program (No. 2019QZKK0201) and the PRIME Laboratory seed program. Harbor's work was supported by Purdue University Global.

Appendix A. Supplementary data

Supplementary data to this article can be found online at https://doi.org/10.1016/j.quascirev.2023.108038.

References

Abramowski, U., Bergau, A., Seebach, D., Zech, R., Glaser, B., Sosin, P., Kubik, P.W., Zech, W., 2006. Pleistocene glaciations of Central Asia: results from ^{10}Be surface exposure ages of erratic boulders from the Pamir (Tajikistan), and the Alay–Turkestan range (Kyrgyzstan). Quat. Sci. Rev. 25, 1080–1096.

Balco, G., 2011. Contributions and unrealized potential contributions of cosmogenic-nuclide exposure dating to glacier chronology, 1990–2010. Quat. Sci. Rev. 30, 3–27.

Balco, G., 2020. Glacier change and paleoclimate applications of cosmogenic-nuclide exposure dating. Annu. Rev. Earth Planet Sci. 48, 21–48.

Balco, G., Stone, J.O., Lifton, N.A., Dunai, T.J., 2008. A complete and easily accessible means of calculating surface exposure ages or erosion rates from ^{10}Be and ^{26}Al measurements. Quat. Geochronol. 3, 174–195.

Batbaatar, J., Gillespie, A.R., Koppes, M., Clark, D.H., Chadwick, O.A., Fink, D., Matmon, A., Rupper, S., 2020. Glacier development in continental climate regions of central Asia. In: Waitt, R.B., Thackray, G.D., Gillespie, A.R. (Eds.), Untangling the Quaternary Period–A Legacy of Stephen C. Porter, vol. 548. Geological Society of America Special Paper, pp. 123–153.

Benn, D.I., Evans, D.J.A., 2010. Glacier and Glaciation, second ed. Hodder Education, London, pp. 1–802.
Benn, D.I., Lehmkuhl, F., 2000. Mass balance and equilibrium-line altitudes of glaciers in high-mountain environments. Quat. Int. 65/66, 15–29.
Benn, D.I., Owen, L.A., 1998. The role of the Indian summer monsoon and the mid–latitude westerlies in Himalayan glaciation: review and speculative discussion. J. Geol. Soc. 155, 353–363.
Bennett, M.R., Glasser, N.F., 2009. Glacial Geology: Ice Sheet and Landforms, second ed. Wiley-Blackwell, Oxford, pp. 1–385.
Berger, A., Loutre, M.F., 1991. Insolation values for the climate of the last 10 million years. Quaternary Science Revtews 10, 297–317.
Bierman, P.R., Marsella, K.A., Patterson, C., Davis, P.T., Caffee, M., 1999. Mid-Pleistocene cosmogenic minimum-age limits for pre-Wisconsinan glacial surfaces in southwestern Minnesota and southern Baffin Island: a multiple nuclide approach. Geomorphology 27, 25–39.
Blomdin, R., Stroeven, A.P., Harbor, J.M., Lifton, N.A., Heyman, J., Gribenski, N., Petrakov, D.A., Caffee, M.W., Ivanov, M.N., Hättestrand, C., Rogozhina, I., Usubaliev, R., 2016. Evaluating the timing of former glacier culmination in the Tian Shan: a key step towards robust spatial correlations. Quat. Sci. Rev. 153, 78–96.
Briner, J.P., Swanson, T.W., 1998. Using inherited cosmogenic ^{36}Cl to constrain glacial erosion rates of the Cordilleran ice sheet. Geology 26, 3–6.
Chen, J., 1989. Preliminary researches on lichenometric chronology of Holocene glacial fluctuations and on other topics in the headwater of Urumqi River, Tianshan Mountains. Science in China (Series B) 32, 1487–1500.
Chen, F.H., Huang, X.Z., Zhang, J.W., Holmes, J.A., Chen, J.H., 2006. Humid Little ice age in arid central Asia documented by Bosten Lake, Xinjiang, China. Sci. China Earth Sci. 49, 1280–1290.
Chen, Y.X., Li, Y.K., Wang, Y.Y., Zhang, M., Cui, Z.J., Yi, C.L., Liu, G.N., 2015. Late Quaternary glacial history of the Karlik Range, easternmost Tian Shan, derived from ^{10}Be surface exposure and optically stimulated luminescence datings. Quat. Sci. Rev. 115, 17–27.
Chen, F.H., Chen, J.H., Huang, W., Chen, S.Q., Huang, X.Z., Jin, L.Y., Jia, J., Zhang, X.J., An, C.B., Zhang, J.W., Zhao, Y., Yu, Z.C., Zhang, R.H., Liu, J.B., Zhou, A.F., Feng, S., 2019. Westerlies Asia and monsoonal Asia: spatiotemporal differences in climate change and possible mechanisms on decadal to sub-orbital timescales. Earth Sci. Rev. 192, 337–354.
Çiner, A., Sarıkaya, M.A., Yıldırım, C., 2015. Late Pleistocene piedmont glaciations in the Eastern Mediterranean; insights from cosmogenic ^{36}Cl dating of hummocky moraines in southern Turkey. Quat. Sci. Rev. 116, 44–56.
Clark, D.H., Bierman, P.R., Larsen, P., 1995. Improving in situ cosmogenic chronometers. Quat. Res. 44, 367–377.
Clark, P.U., Dyke, A.S., Shakun, J.D., Carlson, A.E., Clark, J., Wohlfarth, B., Mitrovica, J.X., Hostetler, S.W., McCabe, A.M., 2009. The last glacial maximum. Science 325, 710–714.
Cuffey, K.M., Paterson, W.S.B., 2010. The Physics of Glaciers, fourth ed. Elsevier, Amsterdam, pp. 1–693.
Dortch, J.M., Owen, L.A., Haneberg, W.C., Caffee, M.W., Dietsch, C., Kamp, U., 2009. Nature and timing of large landslides in the Himalaya and Transhimalaya of northern India. Quat. Sci. Rev. 28, 1037–1054.
Dortch, J.M., Owen, L.A., Caffee, M.W., 2013. Timing and climatic drivers for glaciation across semi-arid western Himalayan-Tibetan orogen. Quat. Sci. Rev. 78, 188–208.
Dortch, J.M., Tomkins, M.D., Saha, S., Murari, M.K., Schoenbohm, L.M., Doug, C., 2022. A tool for the ages: the probabilistic cosmogenic age analysis tool (P-CAAT). Quat. Geochronol. 71, 101323.
Doughty, A.M., Kaplan, M.R., Peltier, C., Barker, S., 2021. A maximum in global glacier extent during MIS 4. Quat. Sci. Rev. 261, 106948.
Ehlers, J., Gibbard, P.L., Hughes, P.D., 2011. Quaternary Glaciations—Extent and Chronology, vol. 15. A Closer Look. Elsevier, Amsterdam, pp. 1–1108.
Embleton, C., King, C.A.M., 1975. Glacial Geomorphology. Edward Arnold, London, pp. 1–573.
Fabel, D., Stroeven, A.P., Harbor, J., Kleman, J., Elmore, D., Fink, D., 2002. Landscape preservation under Fennoscandian ice sheets determined from in situ produced ^{10}Be and ^{26}Al. Earth Planet Sci. Lett. 201, 397–406.
Fabel, D., Harbor, J., Dahms, D., James, A., Elmore, D., Horn, L., Daley, K., Steele, C., 2004. Spatial patterns of glacial erosion at a valley scale derived from terrestrial cosmogenic ^{10}Be and ^{26}Al concentrations in rock. Ann. Assoc. Am. Geogr. 94, 241–255.
Fuchs, M., Owen, L.A., 2008. Luminescence dating of glacial and associated sediments: review, recommendations and future directions. Boreas 37, 636–659.
Gribenski, N., Jansson, K.N., Preusser, F., Harbor, J.M., Stroeven, A.P., Trauerstein, M., Blomdin, R., Heyman, J., Caffee, M.W., Lifton, N.A., Zhang, W., 2018. Re-evaluation of MIS 3 glaciation using cosmogenic radionuclide and single grain luminescence ages, Kanas Valley, Chinese Altai. J. Quat. Sci. 33, 55–67.
Grove, J.M., 2004. Little Ice Ages: Ancient and Modern, second ed. Routledge, London and New York, pp. 1–718.
Guo, W.Q., Liu, S.Y., Xu, J.L., Wu, L.Z., Shangguan, D.H., Yao, X.J., Wei, J.F., Bao, W.J., Yu, P.C., Liu, Q., Jiang, Z.L., 2015. The second Chinese glacier inventory: data, methods and results. J. Glaciol. 61, 357–372.
Herzschuh, U., 2006. Palaeo-moisture evolution in monsoonal Central Asia during the last 50,000 years. Quat. Sci. Rev. 25, 163–178.
Heyman, J., Stroeven, A.P., Harbor, J.M., Caffee, M.W., 2011. Too young or too old: evaluating cosmogenic exposure dating based on an analysis of compiled boulder exposure ages. Earth Planet Sci. Lett. 302, 71–80.
Heyman, J., Applegate, P.J., Blomdin, R., Gribenski, N., Harbor, J.M., Stroeven, A.P., 2016. Boulder height– exposure age relationships from a global glacial ^{10}Be compilation. Quat. Geochronol. 34, 1–11.
Hu, R.J., 1979. Glaciations in the Karlik Mountain, eastern tianshan range (in Chinese). Xinjiang Geography (Arid Land Geography) 2, 69–78.
Hu, R.J., Xu, S.Y., Li, S.Z., 1964. Preliminary study of palaeoglaciation in the Miaoergou River valley, Hami prefecture. In: Proceedings of Glacier and Snow Research in Xinjiang (In Chinese). Science and technology committee of Xinjiang's Publishing House, Urumqi, pp. 43–50.
IPCC, 2013. Climate Change 2013: the Physical Science Basis. Cambridge University Press, Cambridge, pp. 383–464.
Kelly, M.A., Ivy-Ochs, S., Kubik, P.W., von Blanckenburg, F., Schlüchter, C., 2006. Chronology of deglaciation based on ^{10}Be dates of glacial erosional features in the Grimsel Pass region, central Swiss Alps. Boreas 35, 634–643.
Kohl, C.P., Nishiizumi, K., 1992. Chemical isolation of quartz for measurement of in-situ-produced cosmogenic nuclides. Geochem. Cosmochim. Acta 56, 3583–3587.
Kong, P., Fink, D., Na, C.G., Huang, F.X., 2009. Late Quaternary glaciation of the Tianshan, Central Asia, using cosmogenic ^{10}Be surface exposure dating. Quat. Res. 72, 229–233.
Koppes, M., Gillespie, A.R., Burke, R.M., Thompson, S., Stone, J., 2008. Late quaternary glaciation in the Kyrgyz tien Shan. Quat. Sci. Rev. 28, 846–866.
Li, Y.K., 2018. Determining topographic shielding from digital elevation models for cosmogenic nuclide analysis: a GIS model for discrete sample sites. J. Mt. Sci. 15, 939–947.
Li, Y.K., Harbor, J., Stroeven, A.P., Fabel, D., Kleman, J., Fink, D., Caffee, M., Elmore, D., 2005. Ice sheet erosion patterns in valley systems in northern Sweden investigated using cosmogenic nuclides. Earth Surf. Process. Landforms 30, 1039–1049.
Li, Y.K., Liu, G.N., Kong, P., Harbor, J., Chen, Y.X., Caffee, M., 2011. Cosmogenic nuclide constraints on glacial chronology in the source area of the Urumqi River, Tian Shan, China. J. Quat. Sci. 26, 297–304.
Li, Y.K., Liu, G.N., Chen, Y.X., Li, Y.N., Harbor, J., Stroeven, A.P., Caffee, M., Zhang, M., Li, C.C., Cui, Z.J., 2014. Timing and extent of Quaternary glaciations in the Tianger Range, eastern Tian Shan, China, investigated using ^{10}Be surface exposure dating. Quat. Sci. Rev. 98, 7–23.
Li, Y.N., Li, Y.K., Chen, Y.X., Lu, X.Y., 2016a. Presumed Little ice age glacial extent in the eastern tian Shan, China. J. Maps 12 (S1), 71–78.
Li, Y.N., Li, Y.K., Harbor, J., Liu, G.N., Yi, C.L., Caffee, M.W., 2016b. Cosmogenic ^{10}Be constraints on Little ice age glacial advances in the eastern tian Shan, China. Quat. Sci. Rev. 138, 105–118.
Lifton, N., Beel, C., Hättestrand, C., Kassab, C., Rogozhina, I., Heermance, R., Oskin, M., Burbank, D., Blomdin, R., Gribenski, N., Caffee, M., Goehring, B.M., Heyman, J., Ivanov, M., Li, Y.N., Li, Y.K., Petrakov, D., Usubaliev, R., Codilean, A.T., Chen, Y.X., Harbor, J., Stroeven, A.P., 2014a. Constraints on the late Quaternary glacial history of the Inylchek and Sary-Dzaz valleys from in situ cosmogenic ^{10}Be and ^{26}Al, eastern Kyrgyz Tian Shan. Quat. Sci. Rev. 101, 77–90.
Lifton, N., Sato, T., Dunai, T.J., 2014b. Scaling *in situ* cosmogenic nuclide production rates using analytical approximations to atmospheric cosmic-ray fluxes. Earth Planet Sci. Lett. 386, 149–160.
LIGG (Lanzhou Institute of Glaciology and Geocryology, Chinese Academy of Science), 1986. Glacier Inventory of China (III) (Tianshan Mountains: Interior Drainage Area of Scattered Flow in East). Science Press, Beijing, pp. 1–72 (in Chinese).
Lisiecki, L.E., Raymo, M.E., 2005. A Pliocene-Pleistocene stack of 57 globally distributed benthic δ^{18}O records. Paleoceanography 20 (PA1003). https://doi.org/10.1029/2004PA001071.
Liu, S.Y., Yao, X.J., Guo, W.Q., Xu, J.L., Shangguan, D.H., Wei, J.F., Bao, W.J., Wu, L.Z., 2015. The contemporary glaciers in China based on the Second Chinese Glacier Inventory. Acta Geograph. Sin. 70, 3–16.
Liu, R.L., Zhao, J.D., Yin, X.F., 2021. Late Quaternary glacial sequence and landform evolution in the Xiate River valley, Tianshan Mountains, China (in Chinese with English abstract). J. Glaciol. Geocryol. 43, 747–755.
Mischke, S., Zhang, C.J., 2010. Holocene cold events on the Tibetan Plateau. Global Planet. Change 72, 155–163.
Mix, A.C., Bard, E., Schneider, R., 2001. Environmental processes of the ice age: land, oceans, glaciers (EPILOG). Quat. Sci. Rev. 20, 627–657.
Moberg, A., Sonechkin, D.M., Holmgren, K., Datsenko, N.M., Karlén, W., 2005. Highly variable Northern Hemisphere temperatures reconstructed from low- and high-resolution proxy data. Nature 433, 613–617.
Murari, M.K., Owen, L.A., Dortch, J.M., Caffee, M.W., Dietsch, C., Fuchs, M., Haneberg, W.C., Sharma, M.C., Townsend-Small, A., 2014. Timing and climatic drivers for glaciation across monsoon-influenced regions of the Himalayan–Tibetan orogen. Quat. Sci. Rev. 88, 159–182.
Narama, C., Kondo, R., Tsukamoto, S., Kajiura, T., Ormukov, C., Abdrakhmatov, K., 2007. OSL dating of glacial deposits during the last glacial in the terskey-alatoo range, Kyrgyz republic. Quat. Geochronol. 2, 249–254.
Narama, C., Kondo, R., Tsukamoto, S., Kajiura, T., Duishonakunov, M., Abdrakhmatov, K., 2009. Timing of glacier expansion during the last glacial in the inner tien Shan, Kyrgyz republic by OSL dating. Quat. Int. 199, 147–156.
Nishiizumi, K., Winterer, E.L., Kohl, C.P., Klein, J., Middleton, R., Lal, D., Arnold, J.R., 1989. Cosmic ray production rates of ^{26}Al and ^{10}Be in quartz from glacially polished rocks. J. Geophys. Res. 94, 17907–17915.

Nishiizumi, K., Imamura, M., Caffee, M.W., Southon, J.R., Finkel, R.C., McAninch, J., 2007. Absolute calibration of ^{10}Be AMS standards. Nucl. Instrum. Methods Phys. Res. B 258, 403–413.
Ou, X.J., Lai, Z.P., Zhou, S.Z., Chen, R., Zeng, L.H., 2015. Optical dating of young glacial sediments from the source area of the Urumqi River in Tianshan Mountians, northwestern China. Quat. Int. 358, 12–20.
Owen, L.A., Dortch, J.M., 2014. Nature and timing of Quaternary glaciation in the Himalayan-Tibetan orogen. Quat. Sci. Rev. 88, 14–54.
Patton, H., Hubbard, A., Andreassen, K., Winsborrow, M., Stroeven, A.P., 2016. The build-up, configuration, and dynamical sensitivity of the Eurasian ice-sheet complex to Late Weichselian climatic and oceanic forcing. Quat. Sci. Rev. 153, 97–121.
Patton, H., Hubbard, A., Andreassen, K., Auriac, A., Whitehouse, P.L., Stroeven, A.P., Shackleton, C., Winsborrow, M., Heyman, J., Hall, A.M., 2017. Deglaciation of the Eurasian ice sheet complex. Quat. Sci. Rev. 169, 148–172.
Reuther, A.U., Fiebig, M., Ivy-Ochs, S., Kubik, P.W., Reitner, J.M., Jerz, H., Heine, K., 2011. Deglaciation of a large piedmont lobe glacier in comparison with a small mountain glacier– new insight from surface exposure dating. Two studies from SE Germany. E&G Quaternary Science Journal 60, 248–269.
Schaefer, J.M., Denton, G.H., Barrell, D.J.A., Ivy-Ochs, S., Kubik, P.W., Andersen, B.G., Phillips, F.M., Lowell, T.V., Schlüchter, C., 2006. Near-synchronous interhemispheric termination of the last glacial maximum in mid-latitudes. Science 312, 1510–1513.
Schaefer, J.M., Oberholzer, P., Zhao, Z.Z., Ivy-Ochs, S., Wieler, R., Baur, H., Kubik, P.W., Schlüchter, C., 2008. Cosmogenic beryllium-10 and neon-21 dating of late Pleistocene glaciations in Nyalam, monsoonal Himalayas. Quat. Sci. Rev. 27, 295–311.
Shi, Y.F., Yao, T.D., 2002. MIS 3b (54~44ka BP) cold period and glacial advance in middle and low latitudes (In Chinese with English abstract). J. Glaciol. Geocryol. 24, 1–9.
Shi, Y.F., Huang, M.H., Yao, T.D., Deng, Y.X., 2000. Glaciers and Their Environments in China— the Present, Past and Future (In Chinese). Science Press, Beijing, pp. 1–410.
Shi, Y.F., Cui, Z.J., Su, Z., 2006. The Quaternary Glaciations and Environmental Variations in China (In Chinese with English Summary). Hebei Science and Technology Publishing House, Shijiazhuang, pp. 1–618.
Shi, Y.F., Zhao, J.D., Wang, J., 2011. New Understanding of Quaternary Glaciations in China (In Chinese). Shanghai Popular Science Press, Shanghai, pp. 1–213.
Solomina, O.N., Bradley, R.S., Jomelli, V., Geirsdottir, A., Kaufman, D.S., Koch, J., McKay, N.P., Masiokas, M., Miller, G., Nesje, A., Nicolussi, K., Owen, L.A., Putnam, A.E., Wanner, H., Wiles, G., Yang, B., 2016. Glacier fluctuations during the past 2000 years. Quat. Sci. Rev. 149, 61–90.
Sorg, A., Bolch, T., Stoffel, M., Solomina, O., Beniston, M., 2012. Climate change impacts on glaciers and runoff in Tien Shan (Central Asia). Nat. Clim. Change 2, 725–731.
Stroeven, A.P., Hättestrand, C., Heyman, J., Kleman, J., Morén, B.M., 2013. Glacial geomorphology of the tian Shan. J. Maps 9, 505–512.
Thompson, L.G., Yao, T., Davis, M.E., Henderson, K.A., Mosley-Thompson, E., Lin, P.N., Beer, J., Synal, H.A., Cole-Dai, J., Bolzan, J.F., 1997. Tropical climate instability: the last glacial cycle from a Qinghai-Tibetan ice core. Science 276, 1821–1825.
Thompson, L.G., Mosley-Thompson, E., Brecher, H., Davis, M., León, B., Les, D., Lin, P.N., Mashiotta, T., Mountain, K., 2006. Abrupt tropical climate change: past and present. Proc. Natl. Acad. Sci. USA 103, 10536–10543.
Wang, Z.C., 1981. A study on palaeoglaciation in the Tianshan range. In: Xinjiang (Ed.), Geological Society of China and Geological Society of, Collected Papers of Quaternary Geology and Glacial Geology in Xinjiang (In Chinese). Xinjiang People's Publishing House, Urumqi, pp. 91–106.
Wang, S.J., 1986. Glaciations. In: Xinjiang Institute of geography, CAS. In: Evolution of the Tianshan Range (In Chinese). Science Press, Beijing, pp. 80–106.
Wang, J., 2010. Glacial advance in the Qinghai-Tibet Plateau and peripheral mountains during the mid-MIS 3 (In Chinese with English abstract). Quat. Sci. 30, 1055–1065.
Wang, Z.T., Liu, C.H., Wang, Y.S., 1986. Distribution and principal features of glaciers in interior drainage area of scattered flow in East Tianshan Mountains (in Chinese). In: LIGG, C.A.S. (Ed.), Glacier Inventory of China (III) (Tianshan Mountains: Interior Drainage Area of Scattered Flow in East). Science Press, Beijing, pp. 7–17.
Wang, Y.J., Cheng, H., Edwards, R.L., Kong, X.G., Shao, X.H., Chen, S.T., Wu, J.Y., Jiang, X.Y., Wang, X.F., An, Z.S., 2008. Millennial- and orbital-scale changes in the East Asian monsoon over the past 224000 years. Nature 451, 1090–1093.
Wang, P.Y., Li, Z.Q., Zhou, P., Wang, W.B., Jin, S., Li, H.L., Wang, F.T., Yao, H.B., Zhang, H., Wang, L., 2015. Recent changes of two selected glaciers in Hami Prefecture of eastern Xinjiang and their impact on water resources. Quat. Int. 358, 146–152.
Xu, X.K., Kleidon, A., Miller, L., Wang, S.Q., Wang, L.Q., Dong, G.C., 2010. Late Quaternary glaciation in the Tianshan and implications for palaeoclimatic change: a review. Boreas 39, 215–232.
Yan, Q., Owen, L.A., Guo, C.C., Zhang, Z.S., Zhang, J.Z., Wang, H.J., 2023. Widespread glacier advances across the Tian Shan during Marine Isotope Stage 3 not supported by climate-glaciation simulations. Fundamental Research 3, 102–110.
Yang, B., Wang, J.S., Bräuning, A., Dong, Z.B., Esper, J., 2009. Late Holocene climatic and environmental changes in arid central Asia. Quat. Int. 194, 68–78.
Yang, X.H., Zhao, J.D., Han, H., 2019. Study on glacier mass balance in the Karlik range, east Tianshan Mountains, 1972-2016 (in Chinese with English Abstract). J. Glaciol. Geocryol. 41, 1–11.
Yi, C.L., Liu, K.X., Cui, Z.J., Jiao, K.Q., Yao, T.D., He, Y.Q., 2004. AMS radiocarbon dating of late Quaternary glacial landforms, source of the Urumqi River, Tien Shan– a pilot study of ^{14}C dating on inorganic carbon. Quat. Int. 121, 99–107.
Zech, R., 2012. A late Pleistocene glacial chronology from the Kitschi-Kurumdu Valley, Tien Shan (Kyrgyzstan), based on ^{10}Be surface exposure dating. Quat. Res. 77, 281–288.
Zech, R., Glaser, B., Sosin, P., Kubik, P.W., Zech, W., 2005. Evidence for long-lasting landform surface instability on hummocky moraines in the Pamir Mountains (Tajikistan) from ^{10}Be surface exposure dating. Earth Planet Sci. Lett. 237, 453–461.
Zhang, M., Chen, Y.X., Li, Y.K., Liu, G.N., 2016a. Late Quaternary glacial history of the Nalati Range, central Tian Shan, China, investigated using ^{10}Be surface exposure dating. J. Quat. Sci. 31, 659–670.
Zhang, W., Liu, L., Chen, Y.X., Liu, B.B., Harbor, J.M., Cui, Z.J., Liu, R., Liu, X., Zhao, X., 2016b. Late glacial ^{10}Be ages for glacial landforms in the upper region of the Taibai glaciation in the Qinling Mountain range, China. J. Asian Earth Sci. 115, 383–392.
Zhao, J.D., Zhou, S.Z., He, Y.Q., Ye, Y.G., Liu, S.Y., 2006. ESR dating of glacial tills and glaciations in the Urumqi River headwaters, Tianshan Mountains, China. Quat. Int. 144, 61–67.
Zhao, J.D., Zhou, S.Z., Liu, S.Y., He, Y.Q., Xu, L.B., Wang, J., 2007. A preliminary study of the glacier advance in MIS 3b in the western regions of China (In Chinese with English abstract). J. Glaciol. Geocryol. 29, 233–241.
Zhao, J.D., Liu, S.Y., He, Y.Q., Song, Y.G., 2009. Quaternary glacial chronology of the ateaoyinake River valley, tianshan mountains, China. Geomorphology 103, 276–284.
Zhao, J.D., Song, Y.G., King, J.W., Liu, S.Y., Wang, J., Wu, M., 2010. Glacial geomorphology and glacial history of the Muzart River valley, Tianshan range, China. Quat. Sci. Rev. 29, 1453–1463.
Zhao, J.D., Lai, Z.P., Liu, S.Y., Song, Y.G., Li, Z.Q., Yin, X.F., 2012. OSL and ESR dating of glacial deposits and its implications for glacial landform evolution in the Bogeda Peak area, Tianshan range, China. Quat. Geochronol. 10, 237–243.
Zhao, J.D., Wang, J., Harbor, J.M., Liu, S.Y., Yin, X.F., Wu, Y.F., 2015. Quaternary glaciations and glacial landform evolution in the Tailan River valley, Tianshan Range, China. Quat. Int. 358, 2–11.
Zhao, J.D., Liu, R.L., Wang, W.C., Dong, Z.J., Qiu, J.K., Zhang, Y.N., Luo, C.W., 2021. Terrestrial in situ cosmogenic nuclides (TCN) dating targets preparation: a case study of its application in Quaternary glaciations research (In Chinese with English abstract). J. Glaciol. Geocryol. 43, 767–775.
Zhou, S.Z., Jiao, K.Q., Zhao, J.D., Zhang, S.Q., Cui, J.X., Xu, L.B., 2002. Geomorphology of the urümqi River valley and the uplift of the tianshan mountains in quaternary. Science in China (Series D) 45, 961–968.